

Convex Formulation of the Zero Emission Vessel Route Planning Problem

Antti Ritari*, Jani Romanoff, Kari Tammi

Department of Energy and Mechanical Engineering, Aalto University, Espoo, Finland

Abstract

This paper focuses on the zero emission vessel route planning problem, which deals with cost-effective planning of battery-electric vessel services for predetermined routes. Vessel characteristics (including battery capacity), fleet size, cyclic schedule frequencies, sailing leg speeds, and shore charging infrastructure are jointly optimized. The problem is nonlinear and nonconvex in its original form, which makes it intractable for most real-world instances. The conventional approach in the literature is to solve a linear approximation by restricting vessel designs and sailing leg speeds to a small finite set. Contrary to the conventional linearization approach, this paper deals with the nonlinearities directly. We show that the problem exhibits a hidden convex structure uncovered by nonlinear changes of variables. By exploiting the favorable convex form of the transformed problem, we solve it in a few seconds using a free off-the-shelf solver that requires no initial guesses, variable bounds, or parameter tuning. We then easily recover the exact solution to the original nonconvex problem by reversing the variable changes. We provide an open-source implementation of our method.

*Corresponding author

Email address: `antti.ritari@aalto.fi` (Antti Ritari)

Contents

1	Introduction	4
1.1	Zero emission vessel route planning problem	4
1.2	Convex reformulation	4
1.3	Contributions	5
1.4	Organization	6
2	Related work	6
2.1	Optimization with log-convex functions	6
2.2	Convexity properties of vessel design problems	7
2.3	Liner shipping network design	8
2.4	Battery-electric vessel modeling	8
3	Modeling with log-convex functions	9
3.1	Logarithmic transformations	9
3.2	Mixed-integer log-convex optimization	10
3.3	Example problem with two variables	11
3.4	Fitting a log-convex function to data	11
4	Transportation network model	12
4.1	Network structure	13
4.2	Indexing sets	13
4.3	Capacity constraints	14
4.4	Demand constraints	15
4.5	Availability constraints	15
4.6	Transportation service level constraint	16
5	Vessel design model	16
5.1	Weight and buoyancy equilibrium	16
5.2	Cargo capacity	18
5.3	Upright transverse stability	18
5.4	Structural strength	21
5.5	Frictional resistance	22
5.6	Residual resistance	24
5.7	Cell and battery models	25
5.8	Battery capacity degradation	26
5.9	Battery deck arrangement	28

5.10	Weight breakdown	30
6	Problem formulation	32
7	Numerical examples	33
7.1	Transportation network	33
7.2	Cases	33
7.3	Results	38
8	Extensions and variations	40
8.1	Demand scenarios	40
8.2	Flow aggregation	40
8.3	Travel time cost	41
Appendix A	Still water loads	41
Appendix B	Hull girder vertical section modulus	43
Appendix C	Hull girder shear flow	44
Appendix D	Numerical integration of wetted area	45

1. Introduction

1.1. Zero emission vessel route planning problem

The maritime shipping industry is accelerating the search for economically and technically viable zero-emission alternatives to conventional fossil fuels. Electricity generated by renewable sources provides a zero-emission pathway through electrofuels or direct electrification. The latter concept refers to storing electrical energy onboard the vessel using battery energy storage. The well-to-wake efficiency of the direct electrification pathway is at least four times greater compared to the electrofuel pathway (Ueckerdt et al., 2021). The rapid decline in the cost of batteries further promotes the feasibility of the direct electrification pathway. However, the current commercially available lithium-ion cells exhibit at least two orders of magnitude lower volumetric energy density than liquid hydrocarbon fuels (Panasonic, 2024). The added volume and weight of the battery, and the increased energy resupply duration at port, prohibit direct substitution of conventional vessels with battery-electric vessels in all except the shortest routes.

This paper focuses on a particular battery-electric fleet deployment problem in the ro-ro, ro-pax, container feeder, and other short-sea liner shipping segments: the selection of appropriate vessel fleet composition (i.e., vessel design and quantity), service frequency, and sailing leg speeds for a predetermined route plan. Our starting point is a given set of ports, cargo demands between each pair, and a route plan consisting of sequences of sailing legs between ports. We deploy one or more battery-electric vessels to each route to operate on a cyclic schedule. The weekly capacity in each route depends on the capacity of vessels, their speeds in sailing legs, and the number of weekly round-trips. The problem is to minimize the fleet lifecycle cost, subject to a minimum transportation service level constraint. Following Havre et al. (2022), we label this problem the *zero emission vessel route planning problem* (ZEVRPP).

1.2. Convex reformulation

ZEVRPP is a nonlinear and combinatorial optimization problem. Nonlinearity arises from the power laws that govern hydrodynamic, hydrostatic, and structural relationships in vessel design. The number of vessels deployed on a route must be an integer, and similarly, the cyclic schedules require integer-valued round-trip voyage frequency. The literature on battery-electric vessel

fleet design for fixed routes (Havre et al., 2022; Torjuul, 2024), and its extension in network design (Havre et al., 2024), deals with the nonlinearities by linear approximations. These works introduce binary decision variables to select sailing leg speeds and vessel capacities from a set of predetermined values. Since this approach assigns binary decision variables for each sailing leg in each route, the combinatorial search space becomes large. The resulting mixed-integer linear problem is tractable only when the size of the set of different speeds and vessel designs is small. Thus, the linearized problem is a poor approximation of the original nonlinear problem.

In this paper, we model the original nonlinear ZEVRRP. Our approach is to model the ZEVRRP as a log-convex optimization problem, which is a particular type of nonconvex optimization problem (we use *log-convex* for conciseness. However, in a strict technical sense, the problem is mixed-integer log-convex). The favourable structure of a log-convex problem allows a transformation to a convex problem with no loss in fidelity. Since we don't introduce any new integer-valued decision variables, our formulation results in a problem with a small combinatorial search space. As a result, it can be solved fast with arbitrary accuracy by solving a sequence of convex subproblems using a standard free off-the-shelf solver code.

1.3. Contributions

The main contribution of this paper is to demonstrate that we can formulate ZEVRRP as a log-convex problem. Once formulated in this form, we can transform the problem into a convex form and solve it efficiently and reliably using a free off-the-shelf solver. The convex problem formulation brings several advantages over the current approach in the literature that relies on linear approximations. Our formulation allows continuous vessel speed variation at each sailing leg, and exact modeling of the multidomain vessel design problem involving the interaction of hydrostatics, hydrodynamics, structures, and general arrangement.

The fact that we can cast ZEVRRP as a log-convex problem has important practical implications. The availability of extremely fast and reliable solution methods for convex problems means that we can perform extensive exploration of the design space. Route plans, demand scenarios, and battery specifications can be swept over a range of values to study alternative scenarios or points when the plan becomes infeasible or constraints become activated. Since solving a single problem instance takes only a few seconds, the design engineer can quickly complete large sweeps over multiple

parameters. Thus, optimization can be applied at the very beginning of the battery-electric vessel fleet planning process, leading to fewer changes in the latter stages and fewer associated costs.

1.4. Organization

We begin with a brief introduction to log-convex modeling in §3. The method description consists of two subsections. The transportation network modeling is described in §4, while §5 lays out the subdomains in the vessel design problem. The coupling between the network and vessel design models is described in §6. Our numerical examples in §7 consider the design of battery-electric ro-pax vessel services in the northern Baltic Sea. We emphasize that the focus of this paper is not on the particular results of these numerical examples. Instead, we focus on modeling the ZEVRRP in a tractable log-convex form as laid out in §3-6. The reader can access the code and all the data needed to reproduce the results reported in this paper at https://users.aalto.fi/~aritari/convex_zevrpp.html.

2. Related work

2.1. Optimization with log-convex functions

The observation that log-transformation achieves lossless convexification of some nonconvex problems dates back to 60s to the book by Duffin et al. (1967). It then took over three decades before log-convex optimization became a practical engineering tool. The interior-point method class of algorithms allowed efficient numerical solutions of log-transformed convex optimization problems (Nesterov and Nemirovskii, 1994). Domain-specific languages for convex optimization (Diamond and Boyd, 2016) introduced automatic variable transformations. The user specifies the problem in its original nonconvex form, and the software then transforms it to the standard convex cone form and passes it to a solver that implements the interior-point method. Finally, reversal of the variable transformations recovers the optimal values of the original variables from the solution. In addition to these developments, we benefit from recent work that formulates a ruleset for constructing complex log-convex functions in a disciplined way from elementary atomic functions (Agrawal et al., 2019).

Many authors have discovered the favorable log-convex structure in important nonconvex engineering problems, including power control in wireless networks (Chiang et al., 2007), gate sizing in large-scale digital circuits (Boyd

et al., 2005), and aircraft design (Hoburg and Abbeel, 2014). Routing cargo over a maritime transportation network can be considered analogous to transmitting over a wireless multihop network in Chiang et al. (2007) or driving currents through a circuit of logic gates in Boyd et al. (2005). In the latter work, convex modeling of the maximum delay along any path through the circuit applies to the problem of determining the port operation (e.g., charging, onboarding, and loading) that takes the longest. Similarly, the global stress response of a vessel hull can be calculated with the convex beam bending model developed for wingbox structural strength analysis in Hoburg and Abbeel (2014)

2.2. Convexity properties of vessel design problems

The authors' previous work was evidently the first to illustrate the log-convex structure of marine vessel design problems (Ritari et al., 2023). This work modeled a single battery-electric vessel with a given cargo capacity and speed profile. In the present paper, we revise all the vessel design subdomain models in Ritari et al. (2023) and embed them in the route planning model that constitutes the ZEVPP. We summarize the key revisions in the following.

- Closed form expressions are derived for several hydrostatic quantities, including hull displacement volume and buoyancy vector position.
- Longitudinal stability of the vessel is ensured by equalizing the battery system center of gravity with the hull longitudinal center of buoyancy.
- The calculation of the metacenter by the moment integral of the water-plane area enhances the accuracy of the transverse stability condition.
- Residual resistance of the hull is included by fitting log-convex functions to experimental data reported in the literature.
- Hull shear strength is modeled by calculating the hull girder cross-section shear flow due to a vertical shear force.
- A semi-empirical model of a lithium-ion cell capacity degradation is adopted from the literature and applied to calculate the battery system replacement cadence over the lifecycle.

2.3. Liner shipping network design

The design of a fleet and a cyclic schedule for a single route in ZEVVRPP (Havre et al., 2022) is a small part of the more general *liner shipping network design problem* (LSNDP). This problem involves designing a service network of vessels sailing at cyclic schedules. The decisions include the routes and the assignment of vessels to the routes. The service network must have sufficient capacity to transport all the requested cargo.

Rana and Vickson (1991) introduced LSNDP in the context of intercontinental container shipping service design. Later, Christiansen et al. (2020) extended the problem with the transhipment of containers and transit time constraints. These authors formulate LSNDP and its extensions as mixed-integer linear programming problems by restricting vessel designs to pre-determined types and selecting among them with 0/1-variables. Speeds in sailing legs are either fixed or modeled as a linear combination of discrete speed levels.

In this paper, we model a service network similar to LSNDP, but we take the routes as a fixed input. A service consists of a set of sailing legs in a linear sequence of ports. Any service that includes a given pair of ports in its route can transport cargo demand between these ports, thus giving rise to interaction effects between the services. We discard cargo unit transshipments because our model targets the design of ferry services first.

2.4. Battery-electric vessel modeling

Recently, many authors have investigated the limits of the economic range of battery electric vessels (Kersey et al., 2022; Moon et al., 2025). These works estimate the battery-electric vessel propulsion power by scaling the power of a reference combustion engine vessel. The scaling law, known as the *the admiralty formula*, gives the electric vessel propulsion power P_{prop} at speed v and displacement ∇ as

$$P_{\text{prop}} = P_{\text{MCR}} \left(\frac{\nabla}{\nabla_{\text{ref}}} \right)^{\frac{2}{3}} \left(\frac{v}{v_{\text{max}}} \right)^3, \quad (1)$$

where P_{MCR} is the combustion engine power output at design speed v_{max} and displacement ∇_{ref} . As the vessel range and battery size increase, the formula's (1) accuracy suffers because it fails to capture the recursive design relationships of a battery-electric vessel.

The displacement correction due to the battery weight leads to a *weight spiral* effect. The increased energy consumption due to the displacement correction needs to be fed back to the battery sizing and iterated until the coupled system of energy and vertical force balance equations is satisfied. Simultaneously, the battery spaces must extend in the longitudinal or vertical direction. In the former case, a longer hull results in a nonlinear increase in maximum bending moment, plate thickness, and steel weight. Alternatively, the battery space can be extended in the vertical direction, which weakens transverse stability, so a larger waterline breadth must compensate. A larger battery capacity is required because a wide hull is hydrodynamically inefficient.

In this paper, we develop a vessel design model that simultaneously resolves all the coupled subsystem equations. Our designs are guaranteed to satisfy all the fundamental design constraints, even when the batteries weigh more and take more space than a conventional vessel's (with the same cargo capacity) engine and fuel tanks.

3. Modeling with log-convex functions

3.1. Logarithmic transformations

We model the nonlinear relationships governing ZEVPP using *log-convex* functions, a special class of continuous nonlinear functions. Let $f : \mathbb{R}_{++}^n \rightarrow \mathbb{R}_{++}$ denote a (possibly nonconvex) function and $F(u) = \log f(\exp u)$ its nonlinear log-transformation (Agrawal et al., 2019). The function f is called *log-convex* if its log-transformation F is convex. (See Boyd and Vandenberghe (2004) for the mathematical background on convex functions and sets).

With $x \in \mathbb{R}_{++}^n$, a nonconvex optimization problem of the form

$$\begin{aligned} & \text{minimize} && f_0(x) \\ & \text{subject to} && f_i(x) \leq 1, \quad i = 1, \dots, m \end{aligned} \tag{2}$$

is called a *log-convex* optimization problem when f_0, \dots, f_m are log-convex.

We can formulate the original nonconvex problem (2) as the equivalent convex problem

$$\begin{aligned} & \text{minimize} && F_0(u) \\ & \text{subject to} && F_i(u) \leq 0, \quad i = 1, \dots, m, \end{aligned} \tag{3}$$

where $u = \log x$ (applied elementwise). While (2) is difficult to solve or intractable, (3) is easy to solve using a standard off-the-shelf numerical solver. The solution of (2) is then easily recovered from the solution of (3) by applying the variable log-transformations in reverse: $x^* = \exp u^*$ (applied elementwise).

The log-transformation F is not a local approximation of f when f is log-convex. Instead, F is a lossless convex transformation in the entire domain of f . However, the log-transformation is not a universal convexification technique for arbitrary nonlinear relationships. It only applies to nonconvex functions with the particular favourable log-convex form.

A *posynomial* is a particular *log-convex* function of the form

$$f(x) = \sum_{k=1}^K c_k \prod_{i=1}^n x_i^{a_{ik}},$$

where $c_k > 0$ are constant coefficients and $a_i \in \mathbb{R}$ are (possibly negative) constant exponents. The log-transformation of a posynomial gives the *log-sum-exp* convex function

$$\log \sum_{k=1}^K c_k \prod_{i=1}^n x_i^{a_{ik}} = \log \sum_{k=1}^K c_k \exp(a_k^T u) = \log \sum_{k=1}^K \exp(b_k + a_k^T u),$$

where $b_k = \log c_k$. The log-transformation of a posynomial with $K = 1$ (called a *monomial*) gives a linear function. The modeling of ZEVPPP in this paper is based mainly on the posynomial functional form. In a few cases, we use rulesets from [Agrawal et al. \(2019\)](#) to construct more complex log-convex functions.

3.2. Mixed-integer log-convex optimization

A mixed-integer log-convex optimization problem is (2) with the additional constraint that at least one decision variable is a positive integer:

$$\begin{aligned} & \text{minimize} && f_0(x) \\ & \text{subject to} && f_i(x) \leq 1, \quad i = 1, \dots, m \\ & && x_i \in \mathbb{Z}_{\geq 1}, \quad i = 1, \dots, k. \end{aligned} \tag{4}$$

A log-transformation of (4) gives a convex mixed-integer nonlinear problem, which is easy to solve to arbitrary accuracy by solving a sequence of convex subproblems. In this work, we use positive discrete decision variables to model service frequencies and the number of vessels deployed on a route.

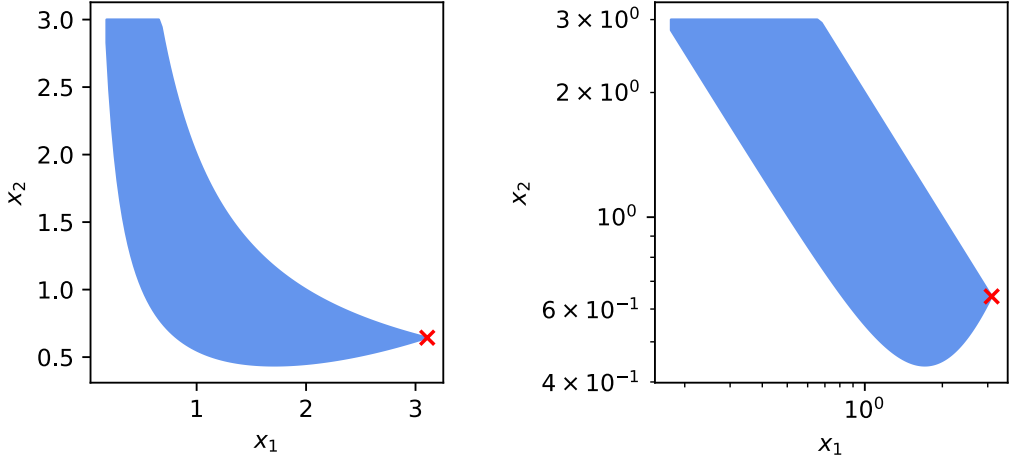


Figure 1: Feasible set of a log-convex optimization problem with two variables. The left panel shows the original nonconvex problem and the right panel shows the log-transformed convex problem. The solid red cross is the optimal solution.

3.3. Example problem with two variables

The following example illustrates convexification via log-transformation. The problem is to minimize a monomial subject to a lower bounding posynomial and two upper bounding monomials with variables $x = (x_1, x_2) \in \mathbb{R}_{++}^2$:

$$\begin{aligned} \text{minimize} \quad & x_1^{-1} \\ \text{subject to} \quad & x_2 \geq 0.5x_1^{-1} + x_1^2/20 \\ & x_2 \leq 2x_1^{-1}, x_2 \leq 3. \end{aligned}$$

Figure 1 draws the feasibility set of the problem in both linear and log-space. The red cross is the global optimum $x^* \approx (3.11, 0.64)$. The constraints define a nonconvex set in linear space but a convex set in log-space.

3.4. Fitting a log-convex function to data

We consider the problem of modeling data generated by sampling a non-log-convex function or a black-box simulation routine. This situation arises when modeling complex physical phenomena like hull hydrodynamics. Our starting point is the N generated data points

$$(x_i, f_i) \in \mathbb{R}_{++}^n \times \mathbb{R}_{++}, i = 1, \dots, N.$$

If we can fit the data with a monomial or a posynomial, the model encoded by the data becomes available in an analytical log-convex functional form.

The fitting problem concerns fitting a convex function to the data points

$$(y_i, g_i) \in \mathbb{R}^n \times \mathbb{R}, i = 1, \dots, N,$$

which have been obtained by the log-transformation $(y_i, g_i) = (\log x_i, \log f_i)$.

Convex functions belonging to the class of *softmax-linear* have been observed to work well in practice with only a small number of terms (Hoburg et al., 2016). This class of functions has the form

$$f_{\text{SMA}}(y) = \frac{1}{\alpha} \log \sum_{k=1}^K \exp(\alpha(b_k + a_k^T y)), \quad (5)$$

where the parameters are $\alpha > 0$, $a_k \in \mathbb{R}^n$ and $b_k \in \mathbb{R}$. The number of user-specified exponential terms is K .

The nonlinear least squares problem seeks the parameters a, b , and α that minimize the sum of squared residuals

$$\text{minimize} \quad \sum_{i=1}^N (f_{\text{SMA}}(y_i, a, b, \alpha) - g_i)^2 \quad (6)$$

with the decision variables a, b and α . Since this is a nonconvex optimization problem, the quality of the fit can depend on the initial guess of the parameters.

The *softmax-linear* function corresponds to the posynomial constraint

$$\sum_{k=1}^K \exp(\alpha b_k) \prod_{i=1}^n x_i^{\alpha a_{ik}} \leq f^\alpha,$$

where the parameters a, b and α are the minimizers of the least squares problem (6).

4. Transportation network model

All the symbols used in §3 are redefined in this and the following sections.

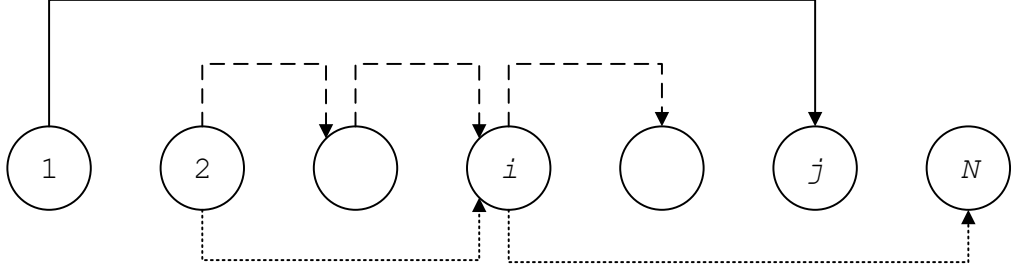


Figure 2: A route is a sequence of sailing legs between linearly ordered ports from 1 to N and indexed by i and j . The figure illustrates a shipping network consisting of three routes constructed from subsets of the same set of N ports. If two or more routes include a pair of ports, multiple services can supply the cargo demand between these ports.

4.1. Network structure

We adopt the notion of a *service*, which is a sequence of ports visited in a regular schedule. One vessel or several identical vessels operate a service. A shipping company typically operates several services among a set of ports in a given geographical area (e.g., the Baltic Sea or the Mediterranean Sea). The demands of cargoes between all pairs of ports are known quantities. The vessels can transport different types of cargoes, e.g., cars, trucks, trailers and passengers, as in the roll-on/roll-off passenger ferry segment. The following notation representing the services and cargo demands builds on the liner network design problem presented by [Christiansen et al. \(2007\)](#).

The ports in the network are linearly ordered and numbered from 1 to N . Each service has two end ports i and j , where $1 \leq i < j \leq N$. A service route starts in i and proceeds outbound to ports with higher and higher numbers until it reaches j . At j , the route turns around and travels inbound to ports with lower and lower numbers until it reaches i . A service with i and j as end ports does not need to call at all ports between i and j . However, the port calls are the same on the route's outbound and inbound legs. Figure 2 illustrates outbound legs of three routes.

4.2. Indexing sets

We let \mathcal{S} be the set of services indexed by s and \mathcal{C} the different types of cargoes indexed by c . Furthermore, let \mathcal{N} be a totally ordered set of the ports 1 to N in a linear order, indexed by i, j, i' and j' . The origin port of

service $s \in \mathcal{S}$ is o_s and the destination port is d_s . The set $\mathcal{N}_s \subseteq \mathcal{N}$ denotes the ports of service $s \in \mathcal{S}$.

The set of ports in service s that precede $i \in \mathcal{N}_s$, and include i , is

$$\mathcal{N}_{is}^- = \{o_s, \dots, i\} \subseteq \mathcal{N}_s$$

and the ports that follow i is the set

$$\mathcal{N}_{is}^+ = \{i, \dots, d_s\} \subseteq \mathcal{N}_s.$$

When a vessel on service s departs from a port $i \in \mathcal{N}_s \setminus d_s$ in the outbound leg, its destination port is the smallest element of the set $\mathcal{N}_{is}^+ \setminus \{i\}$. Let \mathcal{L}_s denote the set of outbound sailing legs in service s according to

$$\mathcal{L}_s = \{(i, j) : i \in \mathcal{N}_s \setminus d_s, j = \min \mathcal{N}_{is}^+ \setminus \{i\}\}.$$

The set of origin-destination demand arcs is

$$\mathcal{A} = \{(i, j) : i \in \mathcal{N}, j \in \mathcal{N}, i \neq j\}.$$

The subset of origin-destination demands supplied by service s is

$$\mathcal{A}_s = \{(i, j) : i \in \mathcal{N}_s, j \in \mathcal{N}_s, i \neq j\} \subseteq \mathcal{A}$$

and the set of services supplying demand for the arc (i, j) is $s : (i, j) \in \mathcal{A}_s$. A vessel on service s departing from port $i \in \mathcal{N}_s$ can supply any demand originating from ports $i' \in \mathcal{N}_{is}^-$ and destined to ports $j \in \mathcal{N}_{is}^+ \setminus \{i\}$.

4.3. Capacity constraints

We let f_{ijcs} , for all $(i, j) \in \mathcal{A}, c \in \mathcal{C}, s \in \mathcal{S}$, denote the decision variable for the quantity of cargo c transported from origin port i to the destination port j by service s during the planning horizon. The transportation capacity of cargo c of a vessel in service s is f_{cs}^{cap} , which is a decision variable governed by constraints specified in the vessel design model introduced in §5. The variable $N_s^{\text{rt}} \in \mathbb{Z}_{\geq 1}, s \in \mathcal{S}$ denotes the number of whole round-trip voyages that a vessel completes in service s during the planning horizon.

The capacity constraints for the outbound legs are written as standard posynomial constraints

$$\sum_{i' \in \mathcal{N}_{is}^-} \sum_{j' \in \mathcal{N}_{is}^+ \setminus \{i\}} f_{i'j'cs} \leq N_s^{\text{rt}} f_{cs}^{\text{cap}} \quad (7)$$

for all $c \in \mathcal{C}$, $s \in \mathcal{S}$, $i \in \mathcal{N}_s \setminus d_s$. For the inbound legs, the capacity constraints take the same form as above, but the departure and arrival ports appear in a reverse order:

$$\sum_{i' \in \mathcal{N}_{is}^-} \sum_{j' \in \mathcal{N}_{is}^+ \setminus \{i\}} f_{j'i'cs} \leq N_s^{\text{rt}} f_{cs}^{\text{cap}}. \quad (8)$$

4.4. Demand constraints

The demand for cargo c on the arc (i, j) over the planning horizon is given by the fixed parameter f_{ijc}^{dem} for all $(i, j) \in \mathcal{A}$, $c \in \mathcal{C}$. The demand on the arc (i, j) is the upper bound on the total quantity of cargo transported by all the services that include these ports in their routes. We write this demand constraint as

$$\sum_{s: (i,j) \in \mathcal{A}_s} f_{ijcs} \leq f_{ijc}^{\text{dem}}, \quad c \in \mathcal{C}, (i, j) \in \mathcal{A}. \quad (9)$$

4.5. Availability constraints

The decision variable v_{ijs} , for all $(i, j) \in \mathcal{L}_s$, $s \in \mathcal{S}$, denotes the sailing speed from port i to j in service s and the parameter l_{ij}^{leg} denotes the sailing distance. The sailing time t_{ijs}^{sea} is the sum of the acceleration time, the deceleration time, and the constant speed sailing time:

$$t_{ijs}^{\text{sea}} = \frac{l_{ij}^{\text{leg}}}{v_{ijs}} + \frac{v_{ijs}}{2} \left(\frac{1}{\dot{v}_s^{(+)}} + \frac{1}{\dot{v}_s^{(-)}} \right),$$

where the acceleration and deceleration rates $\dot{v}_s^{(-)}$ and $\dot{v}_s^{(+)}$ are constant and uniform for each leg in each route.

The cargo loading and unloading times t_{ijsc}^{cl} and t_{ijsc}^{cu} at the destination port of the leg (i, j) in service s for cargo c are given as

$$t_{ijsc}^{\text{cl}} = t_c^{\text{unit}} \sum_{i' \in \mathcal{N}_{js}^- \setminus \{j\}} f_{i'jcs}, \quad t_{ijsc}^{\text{cu}} = t_c^{\text{unit}} \sum_{j' \in \mathcal{N}_{js}^+ \setminus \{j\}} f_{jj'cs},$$

where t_c^{unit} is the loading and unloading duration of a cargo unit c . We let the decision variable t_{ijs}^{cha} for all $(i, j) \in \mathcal{L}_s$, $s \in \mathcal{S}$ denote the charging time at the destination port of the leg (i, j) of a vessel in service s . The docking time t_{ijs}^{port} is then the time of the port operation that takes the longest:

$$t_{ijs}^{\text{port}} = \max\{\max\{t_{ijsc}^{\text{cl}} : c \in \mathcal{C}\}, \max\{t_{ijsc}^{\text{cu}} : c \in \mathcal{C}\}, t_{ijs}^{\text{cha}}\}.$$

Using all the above definitions, we write the availability constraints in the following form, accounting for both the outbound and inbound legs:

$$\sum_{(i,j) \in \mathcal{L}_s} N_s^t(t_{ij}^{\text{sea}} + t_{ji}^{\text{sea}} + t_{ij}^{\text{port}} + t_{ji}^{\text{port}}) \leq t_s^{\text{route}}, \quad s \in \mathcal{S}, \quad (10)$$

where the parameter t_s^{route} is the maximum time a vessel in service s is available during the planning horizon.

4.6. Transportation service level constraint

We require that the transportation network provides a minimum service level:

$$U^{\text{network}} \geq U^{\min}. \quad (11)$$

Here we use *log-utility*, which is a particular concave function with diminishing incremental value of cargo volume shipped in each origin-destination pair and cargo type:

$$\begin{aligned} U^{\text{network}} &= \sum_{(i,j) \in \mathcal{A}} \sum_{s: (i,j) \in \mathcal{A}_s} \sum_{c \in \mathcal{C}} \alpha_{ijc} \log f_{ijcs} \\ &= \log \prod_{(i,j) \in \mathcal{A}} \prod_{s: (i,j) \in \mathcal{A}_s} \prod_{c \in \mathcal{C}} f_{ijcs}^{\alpha_{ijc}}, \end{aligned} \quad (12)$$

where α_{ijc} is a parameter that weights the cargo flows by their arc lengths and cargo value.

5. Vessel design model

This section describes a coupled system of inequalities that captures the key naval-architectural principles governing vessel design. The inequalities are log-convex compatible, meaning we can manipulate them to the form $1 \geq f(x)$, where f is a log-convex function. All the new constraints and the associated design variables hold for each $s \in \mathcal{S}$, but we drop the index for clarity.

5.1. Weight and buoyancy equilibrium

The most elementary design relation states that buoyancy and weight in calm water are in balance because the vessel is a free-floating body. This is expressed as

$$\nabla \rho^{\text{sw}} \geq W_L + W_D, \quad (13)$$

where ∇ is the displaced volume at design draft, ρ^{sw} is the sea water density, and W_L and W_D are lightweight and deadweight in tons. We give a detailed breakdown of the weight in §5.10 and derive a monomial expression for ∇ in the following.

Surfaces defined by closed-form functions describe the submerged hull form. The origin of the coordinate system is located at the foremost point at the keel centerline in a Cartesian coordinate system XYZ . The X -axis points to the port side, the Y -axis points to the direction of the stern, and the Z -axis points upwards. Let $H^{\text{fore}} : \mathbb{R}_+ \times \mathbb{R}_+ \rightarrow \mathbb{R}_+$ and $H^{\text{aft}} : \mathbb{R}_+ \times \mathbb{R}_+ \rightarrow \mathbb{R}_+$ denote two functions that return the lateral offset from the centerline. The particular functions we use are

$$H^{\text{fore}}(y, z) = \frac{B}{2} \sqrt{\frac{2y}{L}} \left(\frac{z}{T} \right)^{1/\beta}, \quad (14)$$

$$H^{\text{aft}}(y, z) = \frac{B}{2} \left(\frac{z}{T} \right)^{1/\beta(1-2y/L)}, \quad y \neq L/2, \quad (15)$$

where L is the length overall, T is the design draft and B is the waterline breadth. All these dimensions are decision variables. In (14) and (15), β is a hull form parameter with a higher value corresponding to a higher block coefficient. Using the above functions, we can describe the half-breadth hull form as a surface in \mathbb{R}^3 as

$$\begin{aligned} & \{(H^{\text{fore}}(y, z), y, z) : 0 \leq y \leq L/2, 0 \leq z \leq T\} \\ & \cup \{(H^{\text{aft}}(y - L/2, z), y, z) : L/2 \leq y < L, 0 \leq z \leq T\}. \end{aligned}$$

Figure 3 illustrates the submerged hull geometry with $\beta = 6$. In this illustration, the hull is extended from the waterline to the topmost continuous deck using the geometry of the forward section.

Displacement volume, wetted surface area, hull steel weight, and buoyant force action point are functions of the variables L, B, T and the form parameter β . The hull displacement volume ∇ at draft T is

$$\begin{aligned} \nabla &= \int_0^{L/2} \int_0^T (H^{\text{fore}}(y, z) + H^{\text{aft}}(y, z)) dz dy \\ &= \underbrace{\left(\frac{1}{2} + \frac{\beta}{3(1+\beta)} - \frac{\log(\beta+1)}{2\beta} \right)}_{C_B} T L B, \end{aligned}$$

where C_B is the block coefficient.

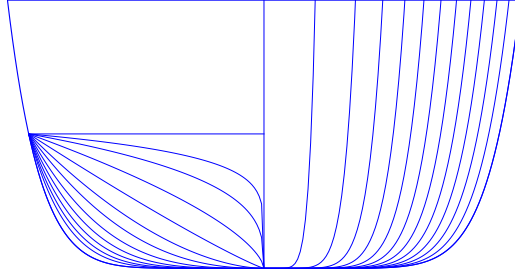


Figure 3: Line drawing of a hull defined by offset functions. The lines represent the intersection of the hull with transverse planes. Lines on the right-hand side of the vertical centerline represent the forward section, and the left-hand side the aft section.

5.2. Cargo capacity

We model mixed-tonnage concept vessels with dedicated spaces for ro-ro cargo and passengers. In our notation, the set \mathcal{C} is $\{\text{pax}, \text{ro-ro}\}$. Here, we don't distinguish between passenger vehicles, trucks, trailers, buses, and other types of ro-ro cargo.

Passengers' accommodation floor area and ro-ro lane capacity are functions of the hull principal dimensions, superstructure length (figure 4), and the number of superstructure decks N^{sup} . The corresponding capacities $f_{c=\text{pax}}^{\text{cap}}$ and $f_{c=\text{ro-ro}}^{\text{cap}}$ are expressed as

$$f_{c=\text{pax}}^{\text{cap}} = \frac{N^{\text{sup}} BL^{\text{sup}}}{\varphi^{\text{pax}}}, \quad f_{c=\text{ro-ro}}^{\text{cap}} = \frac{2BL}{\varphi^{\text{ro-ro}}}.$$

The parameters φ^{pax} and $\varphi^{\text{ro-ro}}$ are unit areas.

5.3. Upright transverse stability

Stability measure calculation relies on the notion of *metacenter*. It is the position on the hull vertical centerline where the buoyancy force vector and the centerline intersect for a small angle of heel. Metacentric height \tilde{h}_{GM} is the vertical distance from the center of gravity to the metacenter:

$$\tilde{h}_{\text{GM}} = \tilde{h}_{\text{KB}} + \tilde{h}_{\text{BM}} - \tilde{h}_{\text{KG}},$$

where \tilde{h}_{KB} is the distance from keel to the center of buoyancy, \tilde{h}_{BM} is the distance from the center of buoyancy to the metacenter and \tilde{h}_{KG} is the distance from keel to the center of gravity (figure 5). The vessel is stable when

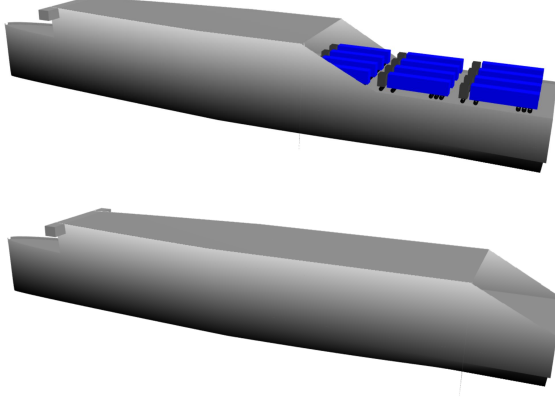


Figure 4: Superstructure length as a design variable. Longer superstructure increases passenger capacity, but also electricity consumption, steel weight, construction cost, and port charges.

$\tilde{h}_{GM} > 0$ by design, meaning the vessel reverts to an upright orientation from a small angle of heel.

The vertical position of the centroid of the displaced water is

$$\begin{aligned}\tilde{h}_{KB} &= \frac{1}{\nabla} \int_0^{L/2} \int_0^T z(H^{\text{fore}}(y, z) + H^{\text{aft}}(y, z)) \, dz \, dy \\ &= \left[\frac{\beta \hat{\beta} \tilde{\beta} / 2 - \hat{\beta} \tilde{\beta} \log \tilde{\beta} / 4 + 2\beta^2 \hat{\beta} / 3}{\beta \hat{\beta} \tilde{\beta} - \hat{\beta} \tilde{\beta} \log \hat{\beta} + 2\beta^2 \tilde{\beta} / 3} \right] T = \beta_{KB} T,\end{aligned}\quad (16)$$

where $\hat{\beta} = \beta + 1$ and $\tilde{\beta} = 2\beta + 1$

The vertical distance from the center of buoyancy to the metacenter is $\tilde{h}_{BM} = I^{WP}/\nabla$, where I^{WP} is the area moment of inertia of the waterplane area about its centroidal axis. We compute the (definite) moment integral

$$I^{WP} = \frac{2}{3} \int_0^{L/2} (H^{\text{fore}}(y, T)^3 + H^{\text{aft}}(y, T)^3) \, dy = \frac{7LB^3}{120},$$

which leads to

$$\tilde{h}_{BM} = \frac{7LB^3}{120C_B LBT} = \frac{7B^2}{120C_B T}.$$

The positive metacentric height requirement for stability follows from the

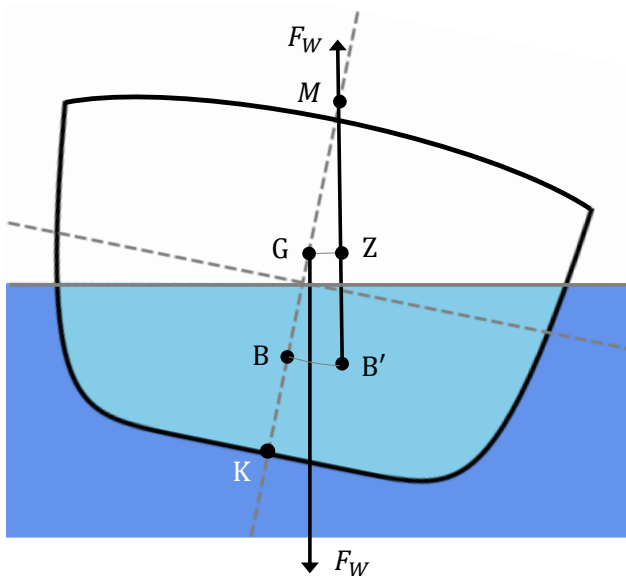


Figure 5: Shifting of center of buoyancy due to heel. The lever arm GZ between buoyancy and weight vectors must be positive by design. Under this condition, the vessel reverts to upright orientation.

quantities defined above as

$$\beta_{\text{KB}}T + \frac{7B^2}{120C_B T} - \tilde{h}_{\text{KG}} \geq \epsilon_{\text{GM}},$$

where ϵ_{GM} is small and positive. Reorganizing the terms gives

$$1 + \frac{7}{120C_B\beta_{\text{KB}}} \left(\frac{B}{T}\right)^2 \geq \frac{\epsilon_{\text{GM}} + \tilde{h}_{\text{KG}}}{\beta_{\text{KB}}T}.$$

This constraint is not a valid log-convex constraint because it imposes a lower bound on a posynomial. We fit a monomial to the posynomial in the relevant range of feasible B/T values (roughly [2.5, 6]) and rewrite the constraint as

$$\delta_1 \left(\frac{B}{T}\right)^{\delta_2} \geq \frac{\epsilon_{\text{GM}} + \tilde{h}_{\text{KG}}}{\beta_{\text{KB}}T}. \quad (17)$$

Here δ_1 and δ_2 are the coefficients of the fitted monomial. The root mean square error is less than 1%.

5.4. Structural strength

The structural strength model ensures that the hull withstands external bending and shear loads without failure. Global structural behavior is the response of the hull to loads acting at the entire length of the hull. At this level, the vessel is modeled as a beam, called *hull girder*, that is loaded with deadweight and lightweight and supported by buoyancy. The properties of the midship cross-section determine the strength of the hull girder.

Figure 6 depicts the hull girder cross-section topology of a ro-pax vessel. The girder extends from the keel to the topmost continuous deck, excluding the superstructure, which does not span the entire length of the hull. Only continuous longitudinal elements of the hull contribute to the structural strength. These include the bottom, inner bottom, side shell, longitudinal bulkheads, and the ro-ro-decks. The elements and their relative positions are fixed, but principal dimensions and plate thicknesses are decision variables whose values determine the strength properties.

An imbalance of buoyancy and weight along the length of the hull creates a bending moment that rises to the maximum value at amidships. We integrate twice the net force per unit length (estimated in [Appendix A](#)), which results in the approximate still water bending moment at amidships:

$$M^{\text{sw}} = 0.0472L^2(C_B + 0.7).$$

A vessel on waves experiences slowly varying buoyancy forces. Classification rules give the formula for the maximum wave bending moment according to the geometry of the hull:

$$M^{\text{wv}} = \varphi^{\text{sh}} 0.975 L^2 B (C_B + 0.7),$$

where $\varphi^{\text{sh}} = -1.1$ for sagging and $\varphi^{\text{sh}} = 1.9 C_B / (C_B + 0.7)$ for hogging. By taking the net design bending moment as $M^{\text{des}} = |M^{\text{wv}}| + |M^{\text{sw}}|$, we can impose the high level bending stress constraint

$$\frac{M^{\text{des}}}{Z^{\text{deck}}} \leq \sigma^{\text{perm}}, \quad (18)$$

where σ^{perm} is the permissible normal stress. The quantity Z^{deck} is a monomial expression for the deck section modulus, which relates the applied moment to the maximum bending stress. It depends on the midship cross-section and is derived in [Appendix B](#).

The still water shear force at the longitudinal coordinate y is obtained from the relation $V^{\text{sw}}(y) = dM^{\text{sw}}(y)/dy$. The wave-induced shear force is

$$V^{\text{wv}}(y) = \varphi_V(y) 0.3 L B (C_B + 0.7),$$

where the value of the coefficient $\varphi_V \in [-0.92, 1]$ varies along the length of the hull. Classification rules give it for both positive and negative shear forces. By taking the still water shear force, and adding to it the contribution from waves, we find the net design shear force $V^{\text{des}} = |V^{\text{sw}}| + |V^{\text{wv}}|$ located at $y = 0.3L$. The corresponding stress limit constraint is

$$|q_{\text{NA}}^{\text{sp}}| \frac{V^{\text{des}}}{p^{\text{sp}}} \leq \tau^{\text{perm}}. \quad (19)$$

Here τ^{perm} is the permissible shear stress. The vertical shear force is mapped to the maximum shear stress response via the quantity $q_{\text{NA}}^{\text{sp}}$, which is a monomial expression for the shear flow at the neutral axis of the side plating. It is derived in [Appendix C](#).

5.5. Frictional resistance

The total vessel resistance R is modeled as a sum of contributions from two sources: frictional resistance R_F and residual resistance R_R . We derive

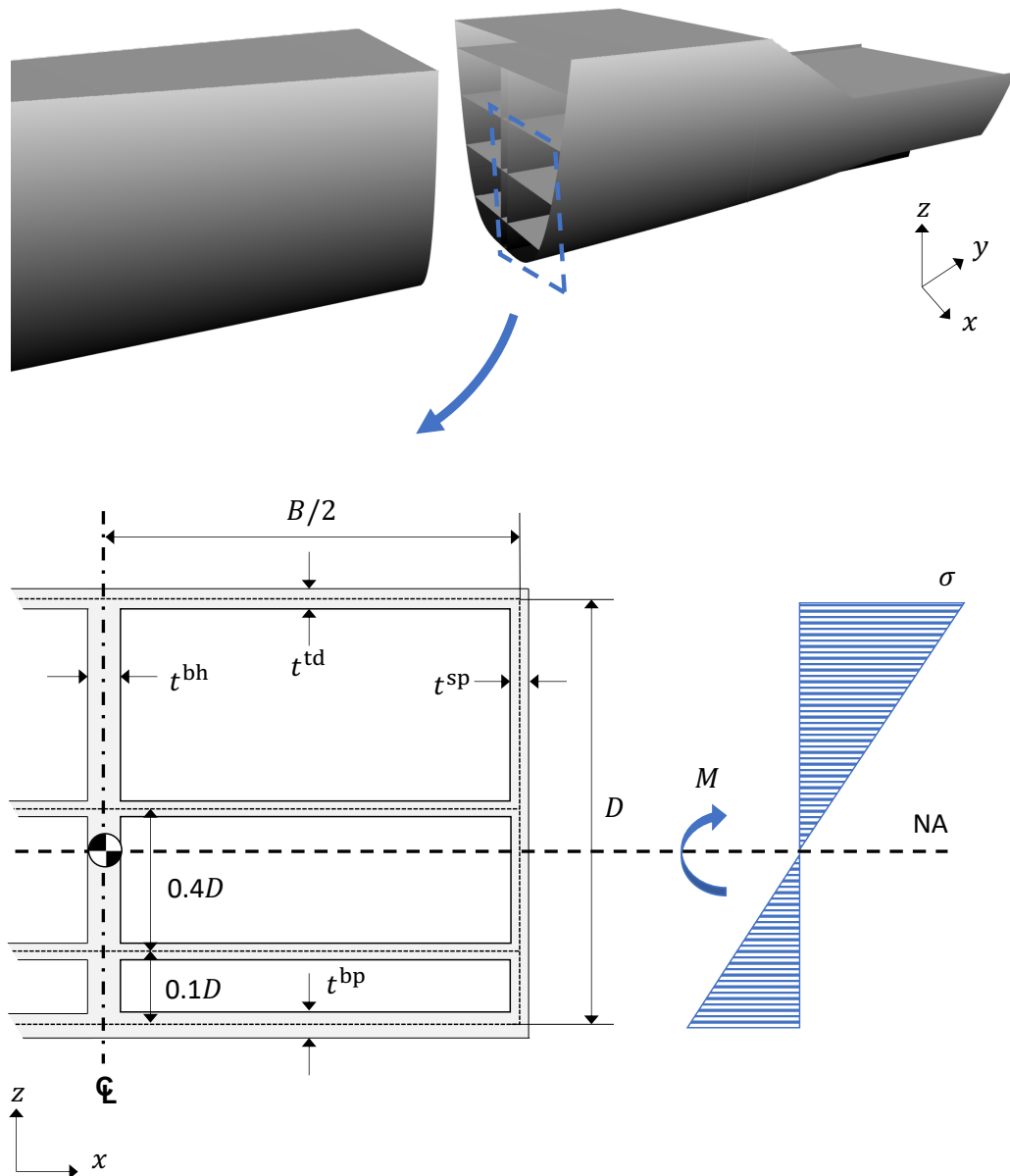


Figure 6: Idealized hull girder cross-section. The normal stress due to vertical bending moment is linearly distributed across the section.

the former component in this section and the latter in §5.6. The total resistance enters into the effective towing power formula in §5.7, which determines the power drawn from the battery along with propeller and power conversion efficiency.

Frictional resistance is

$$R_F = \frac{1}{2} C_F \rho^{\text{sw}} v^2 A_S,$$

where the coefficient C_F can be estimated by the ITTC-57 method via the Reynold's number Re and the kinematic viscosity of water ν :

$$C_F = \frac{75}{(\log_{10}(\text{Re}) - 2)^2}, \quad \text{Re} = \frac{vL}{\nu}.$$

We obtain a log-convex expression for C_F by introducing the auxiliary variable r_{C_F} :

$$C_F = \frac{75}{r_{C_F}^2}, \quad r_{C_F} + 2 \leq \log_{10}(\text{Re}). \quad (20)$$

A numerical integration scheme for calculating the wetted area A_S is described in [Appendix D](#).

5.6. Residual resistance

The residual resistance is given by (note BT as the reference area instead of the wetted surface):

$$R_R = C_R \frac{\rho}{2} v^2 BT.$$

The empirical method by [Hollenbach \(1998\)](#) gives the coefficient C_R for a vessel floating on even keel as

$$C_R = C_R^{\text{std}} C_R^{\text{Fnccrit}} k_L \left(\frac{T}{B} \right)^{\kappa_1} \left(\frac{B}{L} \right)^{\kappa_2} \left(\frac{D_P}{T} \right)^{\kappa_3} (N^{\text{rud}})^{\kappa_4}, \quad (21)$$

where N^{rud} is the number of rudders and $\kappa_1, \dots, \kappa_4$ are constants that depend on the hull type (single or twin-screw configuration). The length dependency factor k_L is the monomial $k_L = \psi_1 L^{\psi_2}$ with constants ψ_1 and ψ_2 .

The standard coefficient C_R^{std} is expressed as a function of the Froude number $\text{Fr} = v/\sqrt{gL}$ with constants $\omega_1, \dots, \omega_9$ as

$$\begin{aligned} C_R^{\text{std}} = & \omega_1 + \omega_2 \text{Fr} + \omega_3 \text{Fr}^2 + C_B (\omega_4 + \omega_5 \text{Fr} + \omega_6 \text{Fr}^2) \\ & + C_B^2 (\omega_7 + \omega_8 \text{Fr} + \omega_9 \text{Fr}^2). \end{aligned} \quad (22)$$

Since the sum $\omega_2 + C_B\omega_5 + C_B^2\omega_8$ is negative according to Hollenbach (1998), (22) cannot be expressed as a log-convex constraint directly. However, we can fit a softmax-affine function (5) to log-transformed data generated with (22) in the relevant Fr range. A fitting function with two exponential terms achieves a sufficiently good fit. The root mean square error is less than 0.1%.

The coefficient $C_R^{\text{Fr}\text{crit}}$ is expressed as

$$C_R^{\text{Fr}\text{crit}} = \max \left\{ 1.0, \left(\frac{\text{Fr}}{\text{Fr}^{\text{crit}}} \right)^{\left(\frac{\text{Fr}}{\text{Fr}^{\text{crit}}} \right)} \right\}, \quad (23)$$

where $\text{Fr}^{\text{crit}} = \theta_1 + \theta_2 C_B + \theta_3 C_B^2$ with constants $\theta_1, \dots, \theta_3$. Since C_B is constant for a given hull form parameter β , Fr^{crit} is also constant.

The second term in the max-function in (23) is not log-convex, because the exponent includes the decision variable Fr. We resolve this by introducing an auxiliary variable r^{Fr} and fitting a posynomial function to data generated from the power function:

$$C_R^{\text{Fr}\text{crit}} \geq \max \{1.0, r^{\text{Fr}}\}, \quad (24)$$

$$(r^{\text{Fr}})^{0.02608} \geq 0.1528\text{Fr}^{1.537} + 0.9672\text{Fr}^{-0.008538}. \quad (25)$$

The fit is excellent, with root mean square error less than 0.01%.

5.7. Cell and battery models

We let b_{ij} denote the battery discharging power on the sailing leg from port i to j . The discharging power is the sum of shaft power and auxiliary power,

$$b_{ij} = P_{ij}^{\text{shaft}} + P_{ij}^{\text{aux}}, \quad b_{ji} = P_{ji}^{\text{shaft}} + P_{ji}^{\text{aux}},$$

for all $(i, j) \in \mathcal{L}$. Here \mathcal{L} is the set of outbound sailing legs of service as described in §4.2. The shaft power is the effective towing power divided by propeller open water efficiency: $P^{\text{shaft}} = (R_F + R_R)v/\eta^{\text{prop}}$.

The battery capacity must be sufficient to supply the energy demand of the sailing leg with the greatest energy consumption. The required energy supply is multiplied by the excess capacity factor Θ and the inverse of discharging efficiency η^{dis} to impose a constraint on the minimum capacity Q as

$$Q \geq \frac{\Theta}{\eta^{\text{dis}}} \max \{ \max \{(bt^{\text{sea}})_{ij}, (bt^{\text{sea}})_{ji}\} : (i, j) \in \mathcal{L} \}. \quad (26)$$

The battery is assembled from N^{cell} number of individual lithium-ion cells with a specified fixed capacity \tilde{Q} and constant voltage V^{cell} . The battery power b , cell current \tilde{b} , battery capacity Q and cell capacity are related according to

$$\tilde{b} = \frac{b}{V^{\text{cell}} N^{\text{cell}}}, \quad \tilde{Q} = \frac{Q}{V^{\text{cell}} N^{\text{cell}}}.$$

We do not track the evolution of the cell charge over consecutive sailing legs. The mean cell charge normalized to its capacity is taken as 50%, i.e., $\tilde{q}/\tilde{Q} = 0.5$ with \tilde{q} denoting the cell charge. This assumption always holds when the capacity factor Θ in (26) is equal to or greater than two.

5.8. Battery capacity degradation

As the battery cycles, its capacity decreases. The battery reaches the end of its lifetime once the capacity drops below some fraction of its initial value (e.g., 80%). We adopt the semi-empirical cell degradation modeling approach in [Suri and Onori \(2016\)](#), which uses a combination of first-principles electrochemistry models and fitting of experimental data.

The fractional capacity loss of a single cell (from its initial capacity) at time t is

$$\phi(t) = [\gamma^{\text{acc}}(t)]^{\chi_1} [\chi_2 + \gamma^{\text{cha}}(t)\chi_3] \exp\left(\frac{-E_A + \chi_4 \gamma^{\text{cur}}(t)}{R_G T^c}\right). \quad (27)$$

The three terms in (27) model the effects of accumulated charge, average charge, and average charge rate.

1. In the first term, $\gamma^{\text{acc}}(t) = \int_0^t |\tilde{b}(\tau)| d\tau$ is the accumulated absolute charge throughput until time t .
2. In the second term, $\gamma^{\text{cha}}(t) = (1/t) \int_0^t (\tilde{q}(\tau)/\tilde{Q}(\tau)) d\tau$ is the average normalized cell charge, which we take as 0.5.
3. The third term originates from the Arrhenius temperature dependence equation. Here $\gamma^{\text{cur}}(t) = (1/t) \int_0^t (|\tilde{b}(\tau)| / \hat{Q}(\tau)) d\tau$ is the average current rate until time t . The constants are activation energy E_A , universal gas constant R_G , and cell temperature T^c .

The parameters χ_1, \dots, χ_4 are identified from cell-dependent experimental data. We use the data from a 3.3V lithium-iron-phosphate cell in [Suri and Onori \(2016\)](#). Figure 7 illustrates the capacity loss of a single cell with varying cycle intensity.

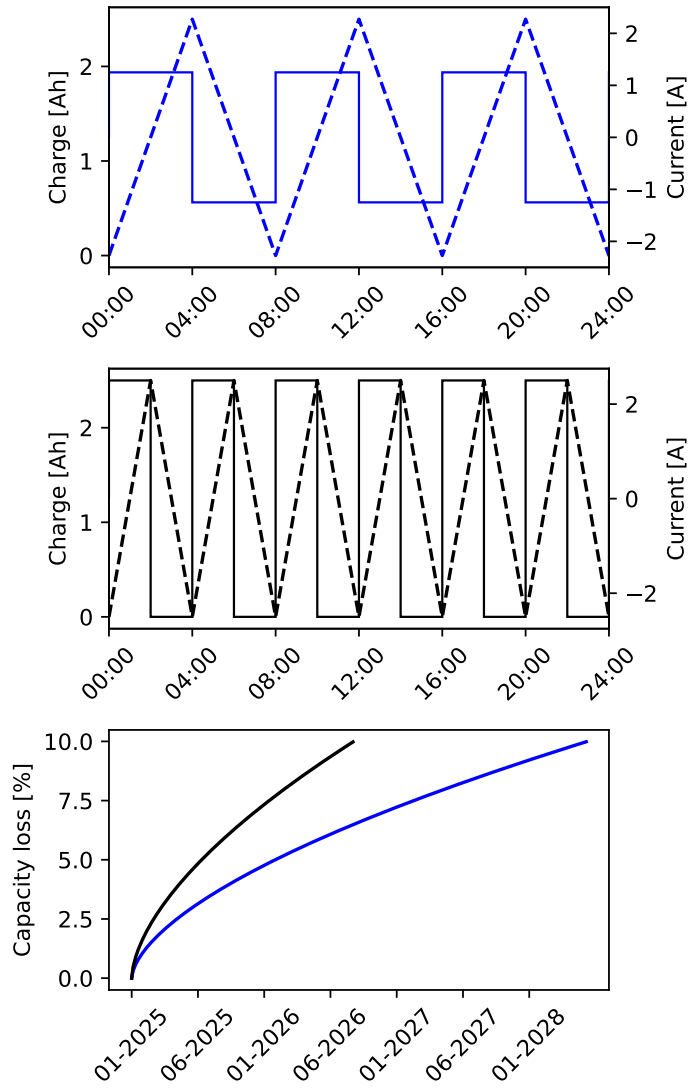


Figure 7: Effect of cycle intensity on cell capacity loss. Three cycles per day (top), six cycles per day (middle), and capacity loss for both charging profiles (bottom).

Since we model the voyage as a set of sequential sailing legs with constant speed, the integrals in (27) take the form of finite sums. We define the auxiliary term r^{dis} and rewrite (27) as the inequality

$$\phi^{\max} \geq (N^{\text{life}} N^{\text{rt}} 2r^{\text{dis}})^{\chi_1} \xi \exp\left(\frac{\chi_4 2N^{\text{rt}} r^{\text{dis}}}{R_G T^{\text{c}} \tilde{Q} t^{\text{ph}}}\right), \quad (28)$$

where

$$\xi = \left(\chi_2 + \frac{1}{2}\chi_3\right) \exp\left(\frac{-E_A}{R_G T^{\text{c}}}\right), \quad r^{\text{dis}} = \sum_{(i,j) \in \mathcal{L}} (\tilde{b}_{ij} t_{ij}^{\text{sea}} + \tilde{b}_{ji} t_{ji}^{\text{sea}}).$$

Here we set the maximum allowed capacity loss to a fixed value ϕ^{\max} and define N^{life} as a decision variable for the number of consecutive planning horizon periods that the battery is used in its lifetime. The constraint (28) is a valid log-convex inequality because the right-hand side is a product of a monomial and a log-convex exp-function.

We let N^{batt} denote the number of complete batteries we need over the vessel's lifetime. Since one battery is always installed for the newbuilding, N^{batt} is defined as

$$N^{\text{batt}} \geq \max\left\{1, \frac{t^{\text{life}}}{N^{\text{ph}} N^{\text{life}}}\right\}, \quad (29)$$

where N^{ph} is the number of planning horizon periods in a year and t^{life} is vessel lifetime in years. The variable N^{life} is used in the cost objective (40) to model the battery investment capital cost.

5.9. Battery deck arrangement

The battery is assembled from many individual modules, stacked vertically in strings and housed in dedicated ventilated rooms. We consider N^{room} uneven number of rooms with the same capacity $Q^{\text{room}} = Q/N^{\text{room}}$. The arrangement is symmetrical about the centermost room (figure 8).

The k th room is specified by its width w_k^{batt} , length l_k^{batt} , equal height h^{batt} , and lower corner $(w_k/2, \tilde{l}_k, \tilde{h})^{\text{batt}}$ in relation to the reference point located at the keel centerline of the forward perpendicular. We impose lower bounds on the room height and elevation from keel:

$$h^{\text{batt}} \geq h^{\text{batt,min}}, \quad (30)$$

$$\tilde{h}^{\text{batt}} \geq 0.1D. \quad (31)$$

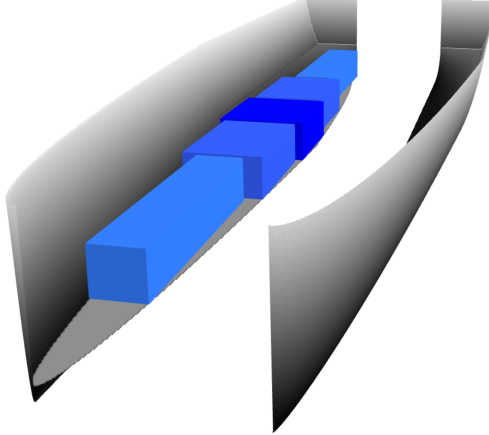


Figure 8: The battery deck is divided into an uneven number of dedicated rooms whose locations and dimensions are design variables. The arrangement is symmetrical about the centermost room. The longitudinal center of gravity is constrained to lie above the hull center of buoyancy.

The room dimensions relate to the volume via monomial equations

$$(w_k h l_k)^{\text{batt}} = Q^{\text{room}} \rho^{\text{vol}}$$

for each $k = 1, \dots, \lceil N^{\text{room}}/2 \rceil$ with $k = 1$ denoting the foremost room. The parameter ρ^{vol} is the volumetric energy density of a battery space.

Each room is enclosed within the hull and prevented from overlapping with adjacent rooms:

$$\frac{w_k^{\text{batt}}}{2} \leq H^{\text{fore}}(\tilde{l}_k^{\text{batt}}, \tilde{h}^{\text{batt}}), \quad k = 1, \dots, \lceil N^{\text{room}}/2 \rceil, \quad (32)$$

$$l_k^{\text{batt}} + \tilde{l}_k^{\text{batt}} \leq \tilde{l}_{k+1}^{\text{batt}}, \quad k = 1, \dots, \lfloor N^{\text{room}}/2 \rfloor. \quad (33)$$

A vessel is designed to float on an even keel by longitudinally aligning the vessel weight and the buoyant force vectors. The position of the centermost room determines the battery center of gravity because the room arrangement is symmetrical. The resulting longitudinal stability constraint is

$$\tilde{l}_{k=\lceil N^{\text{room}}/2 \rceil}^{\text{batt}} + \frac{1}{2} l_{k=\lceil N^{\text{room}}/2 \rceil}^{\text{batt}} \leq \tilde{l}^{\text{cb}}. \quad (34)$$

The inequality is tight because it forces the room position forward from its volume-maximizing position.

The buoyant force acts at the centroid of the displaced water volume. The longitudinal distance of the centroid from the forward perpendicular, denoted \tilde{l}^{cb} in (34), is given by the first moment integral

$$\begin{aligned}\tilde{l}^{\text{cb}} &= \frac{1}{\nabla} \int_0^{L/2} \int_0^T (yH^{\text{fore}}(y, z) + (y+1)H^{\text{aft}}(y, z)) dz dy \\ &= \left[\frac{2\beta^3/(5\hat{\beta}) + 3\beta^2/2 + \beta - \tilde{\beta} \log \hat{\beta}}{2\beta^3/(3\hat{\beta}) + \beta^2 - \beta \log \hat{\beta}} \right] L,\end{aligned}$$

where the parameters $\hat{\beta}$ and $\tilde{\beta}$ are the same as in (16).

The relative positioning constraints of the decks are

$$h^{\text{batt}} + \tilde{h}^{\text{batt}} \leq \tilde{h}^{\text{ro-ro}}, \quad (35)$$

$$T \leq \tilde{h}^{\text{ro-ro}}, \quad (36)$$

$$\tilde{h}^{\text{ro-ro}} + h^{\text{ro-ro}} \leq D. \quad (37)$$

The first two constraints state that the first ro-ro deck is above the battery deck and the waterline. The third constraint specifies vessel depth as the distance from keel to the second ro-ro deck, which we take as the uppermost continuous deck.

5.10. Weight breakdown

Lightweight and deadweight are calculated as

$$\begin{aligned}W_L &= \underbrace{\rho^{\text{st}} \sum_k N_k^{\text{pl}} A_k^{\text{pl}} p_k}_{\text{Structures}} + \underbrace{(0.3L + (L^{\text{sup}})^{3.1} / 10^5) B}_{\text{Outfitting}} \\ &\quad + \underbrace{\rho^{\text{mass}} Q}_{\text{Battery}} + \underbrace{\rho^{\text{mot}} P^{\text{shaft, max}}}_{\text{Motors}},\end{aligned} \quad (38)$$

$$\begin{aligned}W_D &= \underbrace{1565 f_{c=\text{ro-ro}}^{\text{cap}}}_{\text{Ro-ro cargo}} + \underbrace{170(0.02 + 1.146 f_{c=\text{pax}}^{\text{cap}})}_{\text{Passengers and crew}} \\ &\quad + \underbrace{170(0.02 + 1.146 f_{c=\text{pax}}^{\text{cap}})}_{\text{Freshwater}}.\end{aligned} \quad (39)$$

Outfitting weight calculation uses adjusted coefficients from [Watson and Gilligan \(1977\)](#). The basis of calculation for steel weight is the actual or estimated area and thickness of each steel plate element. Table 1 presents posynomial formulas for area calculations and the quantity and thickness of each

Table 1: Surface areas and thicknesses of plate elements.

Plate element	N^{pl}	A^{pl}	p^{pl}
External hull	2	$\varphi_A L l_D^{\text{mid}}$	p^{sp}
Bottom plate	1	$\frac{1}{2} LB$	p^{bp}
Inner bottom	1	$\frac{2}{3} \left(\frac{\tilde{h}^{\text{batt}}}{T} \right)^{1/\beta} BL$	p^{td}
Ro-ro decks	2	$\frac{5}{6} BL$	p^{td}
Ro-ro ramp	1	$B h^{\text{ro-ro}}$	p^{sup}
Longitudinal bulkheads	2	$0.7 LD$	p_{side}
Transverse bulkheads	2	$\sum_{k=1}^{\lceil N^{\text{room}}/2 \rceil} A_k^{\text{tbh}}$	p^{sup}
Walls	2	$\left(2 \sum_{k=1}^{\lfloor N^{\text{room}}/2 \rfloor} l_k^{\text{batt}} + l_{k=\lceil N^{\text{room}}/2 \rceil}^{\text{batt}} \right) h^{\text{batt}}$	p^{sup}
Superstructure	1	$L^{\text{sup}} (6h^{\text{sup}} + 4B + 2h^{\text{ro-ro}}) + B(h^{\text{ro-ro}} + 6h^{\text{sup}})$	p_{sup}

element. The notation A_k^{tbh} refers to the area of the k th transverse bulkhead (extending from keel to battery deck ceiling) defined as

$$A_k^{\text{tbh}} = \int_0^{\tilde{h}^{\text{ro-ro}}} H^{\text{fore}}(\tilde{l}_k^{\text{batt}}, z) dz = \frac{\beta}{\beta + 1} \tilde{h}_k^{\text{ro-ro}} B \left(\frac{\tilde{h}_k^{\text{ro-ro}}}{T} \right)^{1/\beta} \sqrt{\frac{2\tilde{l}_k^{\text{batt}}}{L}}.$$

6. Problem formulation

The ZEVRRP is the problem of minimizing the total fleet cost over a set defined by a system of inequalities from §4 and §5:

minimize	(40)
subject to	Operations
	(7) – (11)
	(13), (17), (34)
	(18), (19)
	(20), (D.4), (D.5), (22), (24), (25)
	(26), (28), (29)
	(30) – (33), (35) – (37)
	Hydrostatics
	Structures
	Hydrodynamics
	Energy
	Dimensions

Table 2 enumerates the decision variables. All the other quantities introduced in §5 are functions of these variables.

The objective function is a sum of annualized investment and operation costs:

$$\begin{aligned}
f^{\text{obj}} = & \sum_{s \in \mathcal{S}} N_s^v \left[\frac{1}{t^{\text{life}}} \left(\underbrace{C_{\text{hotel}}^{\text{pax}} Q_s^{\text{pax}}}_{\text{Hotel crew}} + \underbrace{C_{\text{deck}}^{\text{deck}}}_{\text{Deck crew}} + \underbrace{C^{\text{batt}} N_s^{\text{batt}} k_s^{\text{batt}} E_s^{\text{batt}}}_{\text{Battery}} \right. \right. \\
& + \underbrace{C^{\text{steel}} W_s^{\text{plate}}}_{\text{Hull and outfitting}} \Big) + \sum_{(i,j) \in \mathcal{L}_s} N^{\text{ph}} N_s^t \left(\underbrace{C_j^{\text{port}} V_s^{\text{GT}}}_{\text{Berthing charge}} + \underbrace{C_j^{\text{el}} E_{ijs}^{\text{port}}}_{\text{Electricity}} \right) \Big] \\
& + \frac{1}{t^{\text{life}}} \sum_{i' \in \mathcal{N}} \underbrace{C^{\text{cha}} P_{i'}^{\text{cha}}}_{\text{Chargers}}.
\end{aligned} \tag{40}$$

The port charges are levied in proportion to the vessel's gross tonnage V^{GT} calculated as

$$\begin{aligned}
V^{\text{GT}} = & V^{\text{int}} (0.2 + 0.02 \log_{10}(V^{\text{int}})) \approx V^{\text{int}} 0.2 \\
& + 0.02 \log_{10}(\hat{V}^{\text{int}}) V^{\text{int}} \left(\frac{V^{\text{int}}}{\hat{V}^{\text{int}}} \right)^{1/\log_{10}(\hat{V}^{\text{int}}) \log(10)},
\end{aligned} \tag{41}$$

where V^{int} is the internal volume of the vessel:

$$V^{\text{int}} = C_B^{\text{int}} LBD + N^{\text{sup}} h^{\text{sup}} L^{\text{sup}}.$$

(Here C_B^{int} is an internal volume block coefficient). The last term in (41) replaces the log-function with its local monomial approximation at \hat{V}^{int} . A reasonable choice of \hat{V}^{int} is 10^5 . The error from the approximation is less than 0.1% for typical vessel sizes.

7. Numerical examples

7.1. Transportation network

We model sea transportation services in the northern Baltic Sea region. The route network connects five major ports in Sweden, Estonia, the Finnish mainland, and the autonomous region of the Åland Islands. Connections include both short-distance shuttle services and overnight cruises. Most vessels are ro-pax ferries offering transportation for both ro-ro cargo and passengers. The total number of passengers transported in all the routes was 11.8 million in 2024 (AS Tallink Grupp, 2025). Ro-ro cargo volume, consisting of passenger vehicles, trucks, and trailers, was 2.2 million in the same period.

Conventional combustion engine-powered vessels currently operate all the routes in this region. Fast bunkering of liquid hydrocarbon fuels enables short turnaround times. In particular, the 160 nautical mile route from Turku (Finland) to Stockholm (Sweden) (figure 9) runs on a 24-hour periodic schedule with less than an hour turnaround time in both end ports. Battery-electrification of this route is difficult because the current schedule requires charging powers exceeding 100 megawatts or implementing a battery-swapping scheme.

The other routes' relaxed schedules or short distances make them better suited for electrification. The long-haul overnight routes from Helsinki and Tallinn to Stockholm run on a 48-hour periodic schedule with 7-hour port visits. The flexibility in these routes creates an opportunity to optimize sailing speeds or add a new port call to the service. For example, the Helsinki–Mariehamn–Stockholm vessels can add a 5-hour shuttle service to Tallinn instead of staying berthed continuously for 7 hours at Helsinki.

7.2. Cases

We formulate and solve six instances of the ZEVPP in §6, which are labeled as

B4, U4, M4, M3, M2 and M1.

The letter on the label stands for the fleet type. In the baseline fleet B, the number of vessels and their principal dimensions match the present fleet of

Table 2: Decision variables. We use s to index both services and vessels because all the vessels deployed on a service are identical.

Symbol	Description
f_{ijs}	Quantity of cargo c transported from port i to port j by service s during the planning horizon
v_{ijs}	Sailing speed in leg (i, j) in service s
t_{ijs}^{port}	Turnaround time at the destination port of sailing leg (i, j) in service s
L_s	Hull length of vessel s
L_s^{sup}	Superstructure length of vessel s
B_s	Hull waterline breadth of vessel s
T_s	Draft of vessel s
D_s	Depth of vessel s
p_s	Deck plate thickness of vessel s
h_s^{batt}	Battery room height in vessel s
w_{ks}^{batt}	Width of battery room k in vessel s
l_{ks}^{batt}	Length of battery room k in vessel s
$\tilde{h}_s^{\text{batt}}$	Battery room floor elevation from keel in vessel s
$\tilde{l}_{ks}^{\text{batt}}$	Battery room k front wall distance from forward perpendicular in vessel s
$\tilde{h}_s^{\text{roro}}$	First ro-ro deck elevation from keel in vessel s
E_s^{batt}	Battery capacity of vessel s
t_s^{cell}	Cell cycle life in vessel s
N_s^{batt}	Number of battery replacements in vessel s
P_i^{cha}	Charger power at port i
r_{ijs}^{Cr}	Auxiliary variable for modeling frictional resistance in sailing leg (i, j) in service s
$r_{ijs}^{\text{Cr, std}}$	Auxiliary variable for modeling residual resistance in sailing leg (i, j) in service s
$r_{k's}^g$	Auxiliary variable for point k' in the numerical integration of hull wetted area of vessel s
$r_{k's}^{g2}$	Auxiliary variable for point k' in the numerical integration of hull steel area of vessel s
N_s^{rt}	Frequency of service s
N_s^{vessel}	Number of vessels deployed in service s

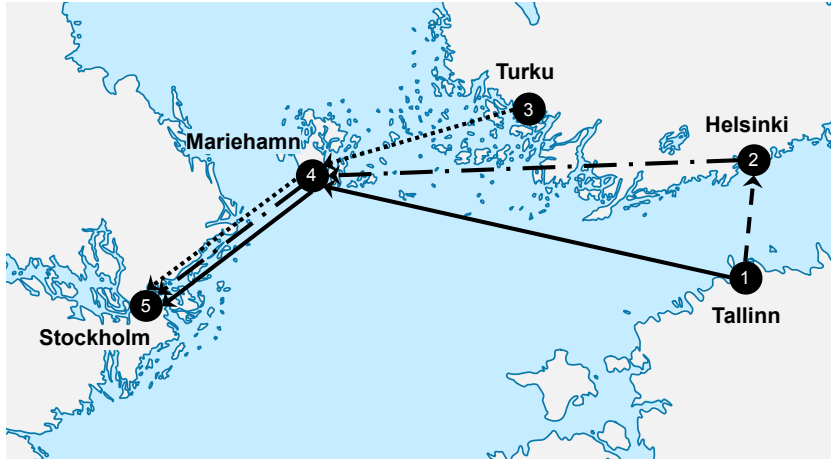


Figure 9: Northern Baltic Sea ferry service route plan with four routes.

the largest ferry operator in the region. Moreover, we assign the services the same frequencies currently used in the routes. The uniform fleet U consists of interchangeable vessels of the same optimized design allocated for all the routes. The mixed fleet M is assembled from vessels optimized for each route.

The number in the label represents the number of distinct routes in the transportation network. Figure 9 illustrates the current network of four routes. The first alternative network in figure 10 routes traffic from Estonia to Sweden via Finland, eliminating one route. The number of routes is further reduced to two and one while preserving a direct connection between all the mainland ports (figures 11 and 12). In all the alternative networks, vessels in service to and from Sweden call at the Åland Islands to benefit from tax exemption, which enables duty-free sales on board.

We use CVXPY (Diamond and Boyd, 2016) modeling language to represent the problem instances and solve them with the primal-dual interior point algorithm implemented in the solver ECOS (Domahidi et al., 2013). The branch and bound extension handles the integer-valued decision variables. The solver obtains the global optimum in less than 10 seconds on a standard desktop computer in all the problem instances. Table 3 shows the demand input data (the same for all problem instances) for every active origin-destination port pair. The other fixed parameter values can be accessed in the implementation code (see §1.4).

Table 3: 48-hour demands between each port-pair $(i, j) : i \in \mathcal{N}, j \in \mathcal{N}, i \neq j$. The data are given in the format *passengers (cargo)*. One unit is a thousand lane-meters or a thousand passengers. The demand is estimated from route-specific traffic volumes and market shares reported in [AS Tallink Grupp \(2025\)](#)

i/j	1	2	3	4	5
1	-	20.50	-	0.05	1.72
		(47.92)	-	(0.01)	(3.00)
2	20.50	-	-	0.1	4.56
	(47.92)	-	-	(0.02)	(2.21)
3	-	-	-	1.36	6.10
	-	-	-	(0.25)	(19.85)
4	0.05	0.1	1.36	-	1.71
	(0.01)	(0.02)	(0.25)	-	(0.32)
5	1.72	4.56	6.10	1.71	-
	(3.00)	(2.71)	(19.85)	(0.32)	-



Figure 10: Northern Baltic Sea ferry service route plan with three routes.

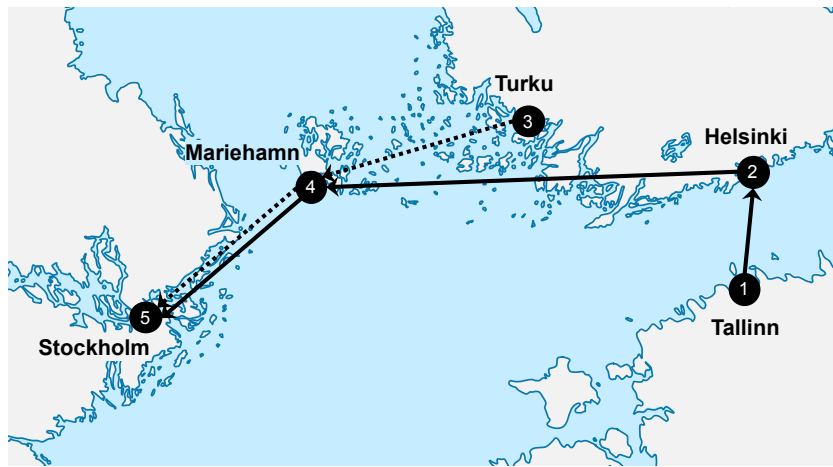


Figure 11: Northern Baltic Sea ferry service route plan with two routes.



Figure 12: Northern Baltic Sea ferry service route plan with a single route.

Table 4: Optimal values of selected fleet design variables. The annual total fleet cost in millions of EUR is displayed in brackets below the case label.

Case	Route	N^{rt}	N^{vessel}	L	L^{sup}	V^{GT}	E^{batt}	t^{cell}
				[m]	[m]	10^3	[MWh]	[a]
B4	12	6	3	212	191	43.6	38.9	2.1
	(216.4)	145	1	2	212	191	55.3	82.8
		245	1	2	203	183	50.4	81.6
		345	2	1	212	191	58.9	62.3
U4	12	6	1	161	130	21.9	101.6	17.0
	(114.5)	145	2	1	161	130	21.9	101.6
		245	2	2	161	130	21.9	101.6
		345	2	3	161	130	21.9	101.6
M4	12	6	1	109	83	11.1	13.1	1.6
	(106.6)	145	2	1	200	101	30.3	131.6
		245	2	1	223	202	54.4	163.6
		345	2	3	133	119	18.7	24.8
M3	12	4	1	96	63	9.9	5.7	3.6
	(103.8)	1245	2	2	185	167	32.8	197.1
		345	2	2	141	127	21.8	24.5
M2	1245	2	2	210	150	36.8	224.2	4.3
	(120.7)	345	2	3	143	120	22.0	24.8
M1	12345	1	14	166	107	20.5	60.3	6.7
	(193.8)							

7.3. Results

Tables 4 and 5 shows optimal values of selected fleet design and operation variables, while table 6 shows the optimal port charger powers. Comparing the solutions for cases B4 and M4, we see that an optimized fleet more than halves the fleet cost compared to the present fleet in the same 4-route network. M4 deploys smaller ships to the short routes and a smaller overall fleet size. On the other hand, two routes operate at a higher frequency, enabled by higher speeds and shorter turnaround times. In the Helsinki-Tallinn route, M4 maintains the same frequency as B4, but manages to reduce speed by optimizing the port turnaround times. The vessel deployed to the cargo-heavy Tallinn-Helsinki route features a short superstructure, which saves building cost, electricity, and port charges.

Table 5: Optimal values of selected fleet operation variables. Sailing leg speeds are in the order they appear in the outbound voyage. The value in the brackets is the speed of the same sailing leg in the inbound voyage.

Case	Route	v_1 [kn]	v_2 [kn]	v_3 [kn]	v_4 [kn]
B4	12	21.6 (21.6)	-	-	-
	145	14.9 (15.0)	15.6 (15.3)	-	-
	245	15.1 (15.1)	15.6 (15.5)	-	-
	345	15.7 (15.6)	15.7 (15.8)	-	-
U4	12	16.0 (16.0)	-	-	-
	145	21.2 (21.3)	23.1 (23.7)	-	-
	245	21.2 (21.2)	23.1 (22.8)	-	-
	345	14.3 (14.2)	14.3 (14.2)	-	-
M4	12	15.1 (15.1)	-	-	-
	145	21.8 (21.7)	22.7 (22.8)	-	-
	245	22.3 (22.3)	23.3 (23.2)	-	-
	345	14.2 (14.1)	14.4 (14.4)	-	-
M3	12	10.0 (10.0)	-	-	-
	1245	27.6 (27.2)	25.6 (25.6)	27.2 (27.0)	-
	345	13.9 (13.9)	14.6 (14.6)	-	-
M2	1245	27.7 (27.3)	25.9 (25.9)	27.3 (27.1)	-
	345	13.9 (13.8)	14.5 (14.5)	-	-
M1	12345	17.5 (17.5)	16.1 (16.1)	17.5 (17.5)	17.5 (17.5)

Table 6: Optimal shore charger powers in megawatts.

Case	1	2	3	4	5
B4	8.9	8.9	21.2	77.5	21.0
U4	75.5	59.1	8.6	131.0	56.7
M4	79.2	89.9	9.47	164.3	54.0
M3	27.1	133.6	11.2	182.8	49.3
M2	23.5	149.1	9.5	202.2	42.7
M1	3.0	19.1	29.8	26.7	5.2

Deploying a uniform fleet to the 4-route network is only 7.4% more expensive than an optimized fleet (cases U4 and M4). This result is surprising considering that the gross tonnage of the largest vessel in M4 is almost five times larger than the gross tonnage of the smallest vessel. In U4, the batteries are vastly oversized in the short routes. However, the oversizing also brings low cycling load and long lifetime.

The 3-route network modeled in the case M3 achieves the lowest cost among all the cases, which indicates that the currently used 4-route network is suboptimal. The basic idea in the 3-route network is to reduce fleet size by combining the routes originating from Tallinn and Helsinki to Stockholm. Simultaneously, the new combined route brings additional capacity to the Tallinn-Helsinki route. The port of Tallinn is equipped with a smaller charger because the frequency of the Helsinki-Tallinn drops from three daily round-trips to two. Finally, the single and 2-route networks M1 and M2 show poor performance because they supply reduced capacity to the high-demand Helsinki-Tallinn route.

8. Extensions and variations

8.1. Demand scenarios

Demand for maritime transportation services varies daily, weekly, and monthly. For example, the monthly passenger traffic volume in the northern Baltic Sea is three times greater in the summer holiday season compared to mid-winter (Statistics Finland, 2025). Incorporating demand scenarios into the problem formulation in §6 is straightforward by introducing indexing of the operational decision variables by the demand scenarios. This extension costs many new decision variables and constraints, including the discrete service frequency variables. However, the problem decomposes into smaller scenario-specific subproblems, only coupled by the fleet design variables. Specialized solution methods can leverage this property.

8.2. Flow aggregation

The log-sum function (12) assigns a different utility for a transportation volume depending on the number of services that deliver that volume between an origin-destination port pair. Specifically, the formulation favors a larger number of services. An alternative approach is to calculate the utility from the aggregate flow from all the services. The constraints that aggregate

the flows impose a lower bound on posynomials, which destroys the favorable log-convex structure. In [Boyd et al. \(2007\)](#) (§9.1), the authors suggest a sequential local solution method that involves taking local monomial approximations of the lower-bounded posynomials. They observe that this method works well in practice.

8.3. Travel time cost

Thus far, we have ignored that the demand between a given origin-destination port pair is not fixed, but depends on the transportation service's availability and characteristics. Passenger ferry services compete with low-cost airlines, and ro-ro cargo can use (at least in some cases) alternative land-based routes. To ensure that the new battery-electric ferry fleet offers competitive travel times, we can extend the cost-objective (40) with a travel time term. Since the total travel time on a route is a posynomial expression of sailing leg speeds, the travel time terms preserve the favorable log-convex structure.

Appendix A. Still water loads

The top two panels in figure A.13 illustrate buoyancy and weight per unit length of the hull in §5.1 floating with static draft at even keel. The local buoyancy force per unit length equals the local hull submerged cross-sectional area. The weight distribution is the sum of distributions of the weight components (38) and (39), assuming $L^{\text{sup}}/L = 0.8$, $N^{\text{room}} = 3$ and $l_k^{\text{batt}}/L = 0.23$. The middle panel in figure A.13 shows the imbalance of the distributions along the length of the hull. This imbalance causes shear force and bending moment at each hull cross-section.

Let $W(y)$ and $\nabla(y)$ denote the unit length weight and buoyancy at the longitudinal coordinate y . The still water shear force $V^{\text{sw}}(y)$ and bending moment $M^{\text{sw}}(y)$ lengthwise distributions are given by the integrals

$$V^{\text{sw}}(y) = \int_0^y (W(\tilde{y}) - \nabla(\tilde{y})) d\tilde{y}, \quad M^{\text{sw}}(y) = \int_0^y V^{\text{sw}}(\tilde{y}) d\tilde{y}.$$

The resulting forces and moments per unit length are illustrated in the bottom two panels in figure A.13.

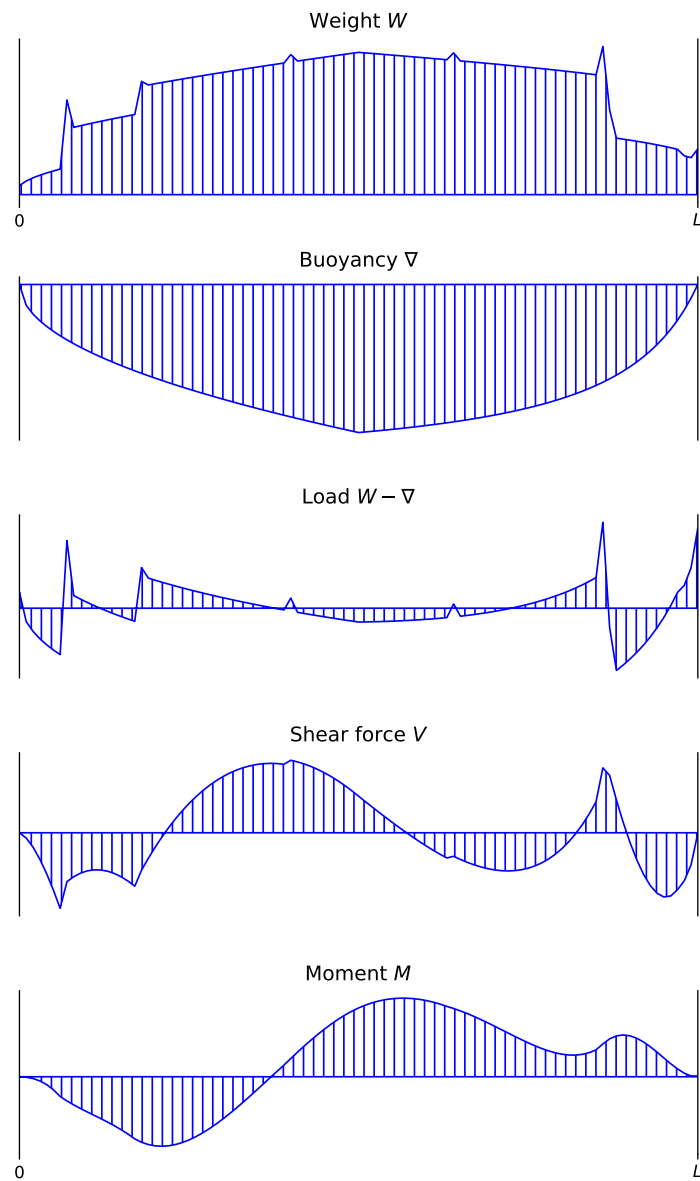


Figure A.13: Weight, buoyancy forces and the resulting still water loads. The origin of the coordinate system is at the forward perpendicular.

Appendix B. Hull girder vertical section modulus

Normal stress $\sigma(z)$ at a vertical distance z from the reference line relates to the bending moment M as

$$\sigma(z) = \frac{M}{\tilde{I}}(z - \tilde{z}_{\text{NA}}),$$

where \tilde{I} is a geometrical property of the cross-section, called the *moment of inertia* about the girder neutral axis \tilde{z}_{NA} . The section modulus $Z = \tilde{I}/(z - \tilde{z}_{\text{NA}})$ in relation to the structural element with the highest stress defines the ultimate strength of the hull girder.

The section modulus is a function of the principal dimensions and thicknesses of the structural elements of the hull girder illustrated in figure 6. The structural components are the bottom, inner bottom, first ro-ro deck, topmost continuous deck (i.e., second ro-ro deck), side shell, and longitudinal bulkheads. We model the two adjacent longitudinal bulkheads as a single bulkhead with double thickness.

The thicknesses of the side shell plates, lumped bulkhead, and bottom relate to the topmost deck according to the fixed ratios

$$p^{\text{sp}} = \frac{Bp^{\text{td}}}{2D}, \quad p^{\text{bh}} = 2p^{\text{sp}} \quad \text{and} \quad p^{\text{bp}} = \frac{2}{3}p^{\text{td}}.$$

The vertical position of the cross-section neutral axis from the reference is the vertical coordinate of the cross-section centroid, defined as

$$\tilde{z}_{\text{NA}} = \frac{\sum_i N_i (z_{\text{NA}})_i A_i}{\sum_i N_i A_i} = \frac{2}{5}D,$$

where the structural elements are indexed by i . The quantity N_i , neutral axis coordinate $(z_{\text{NA}})_i$ and area A_i of each element are given in table B.7.

The second moment of area of the cross-section is calculated using the parallel axis theorem according to

$$\begin{aligned} \tilde{I} &= \sum_i (I_i + A_i(z_{\text{NA}} - \tilde{z}_{\text{NA}})_i^2) = \sum_i \left(\frac{w_i h_i^3}{12} + w_i h_i (z_{\text{NA}} - \tilde{z}_{\text{NA}})_i^2 \right) \\ &\approx \frac{133}{150} p^{\text{td}} BD^2, \end{aligned} \tag{B.1}$$

where w_i is the width of the i th element, h_i is the height, and $I_i = w_i h_i^3/12$ is the second moment of area of the element with respect to its own centroid. In

Table B.7: Properties of the midship cross-section structural elements.

Element	N	w	h	A	z_{NA}	$z_{NA} - \tilde{z}_{NA}$
Bottom	1	B	$3p^{td}/2$	$3Bp^{td}/2$	0	$-2D/5$
Inner bottom	1	B	p^{td}	Bp^{td}	$D/10$	$-3D/10$
Ro-ro deck	1	B	p^{td}	Bp^{td}	$D/2$	$D/10$
Top deck	1	B	p^{td}	Bp^{td}	D	$3D/5$
Side plate	2	p^{sp}	D	$Bp^{td}/2$	$D/2$	$D/10$
Bulkhead	1	p^{sp}	D	Bp^{td}	$D/2$	$D/10$

(B.1), we use the approximation $I_i \approx 0$ for all the deck and bottom elements. The second moment of area of a thin-walled horizontal element, about its own neutral axis, is sufficiently small to be negligible.

Since $\tilde{z}_{NA} < D/2$, the distance from the cross-section neutral axis to the girder top deck is larger than the distance to the bottom. The section modulus at the top deck is lower than at the bottom, which implies that the maximum normal stress is at the deck. The deck section modulus is

$$Z^{\text{deck}} = \frac{5\tilde{I}}{3D}.$$

Appendix C. Hull girder shear flow

The vertical shear force V induces a shear stress τ in the hull girder. The shear force is equal to the shear stress integrated over the area of the cross-section. The shear stress distribution in a thin-walled cross-section is determined using *shear stress flow* $q = p\tau$. We let s denote a coordinate running along the cross-section. Shear flow per unit shear force at s is

$$q(s) = q_0 - \frac{1}{\tilde{I}} \int_0^s (z(s) - \tilde{z}_{NA}) p(s) ds, \quad (\text{C.1})$$

where q_0 is the shear flow at the starting point of the integration (Varsta et al., 2017).

The coordinates where $q(s) = 0$ are indeterminate in a cross-section of one or more closed cells. When the starting point of the shear flow integration in (C.1) (with $q_0 = 0$) is arbitrary, discontinuities in the longitudinal displacement $u(s)$ may occur. The discontinuities need to be compensated by adding constant shear flows along the walls of all the closed cells until the

integration of the longitudinal displacement is zero along the circumference of each cell:

$$\oint_{\text{cell}} u(s) ds = -\frac{1}{G} \oint_{\text{cell}} \frac{q(s)}{p(s)} ds = 0.$$

(Here G is the shear modulus). For the details of this compensation procedure, see §5 in [Varsta et al. \(2017\)](#) or §6.3 in [Mittelstedt \(2021\)](#). The symmetry properties of the hull girder cross-section result in zero shear flows at the half-section vertical centerline of each horizontal element, as illustrated in figure [C.14](#).

The hull girder cross-section is symmetrical with respect to the skeleton line of the bulkhead, and the bulkhead is twice as thick as the side shell plates. Therefore, the same maximum shear stress value occurs at the neutral axis of both elements. In the following, we use the maximum shear flow value at the side shell plates to determine the ultimate stress.

The shear flow [\(C.1\)](#) at the end node j of a constant thickness straight line segment from node i to j is

$$q_j = -\frac{pl}{2\tilde{I}}(z_j + z_i - 2\tilde{z}_{\text{NA}}) + q_i, \quad (\text{C.2})$$

where z_i, z_j are the z -coordinates (from baseline) of the nodes i, j , the length of the line segment is l and q_i is the shear flow at node i ([Lloyd's Register, 2023](#)). Using nodes from A to E (figure [C.14](#)) and four line segments defined in table [C.8](#), we find the maximum shear flow per unit shear force

$$q_E = -\frac{53BDp^{\text{dp}}}{200\tilde{I}}$$

as a function of the midship cross-section principal dimensions and the deck plate thickness.

Appendix D. Numerical integration of wetted area

The wetted area is the surface integral

$$A_S = 2 \int_0^{L/2} \int_0^T \left(\left\| \begin{bmatrix} -\frac{\partial H^{\text{fore}}}{\partial y} \\ -\frac{\partial H^{\text{fore}}}{\partial z} \\ 1 \end{bmatrix} \right\| + \left\| \begin{bmatrix} -\frac{\partial H^{\text{aft}}}{\partial y} \\ -\frac{\partial H^{\text{aft}}}{\partial z} \\ 1 \end{bmatrix} \right\| \right) dz dy,$$

Table C.8: Properties of the hull girder cross-section line segments.

Element	i	j	l	p	z_i	z_j	q_i
Top deck	A	B	$B/4$	p^{td}	D	D	0
Side shell	B	D	$D/2$	p^{sp}	D	$D/2$	$q_{A \rightarrow B}$
Ro-ro deck	C	D	$B/4$	p^{td}	$D/2$	$D/2$	0
Side shell	D	E	$D/10$	p^{sp}	$D/2$	$2D/5$	$q_{A \rightarrow D} + q_{C \rightarrow D}$

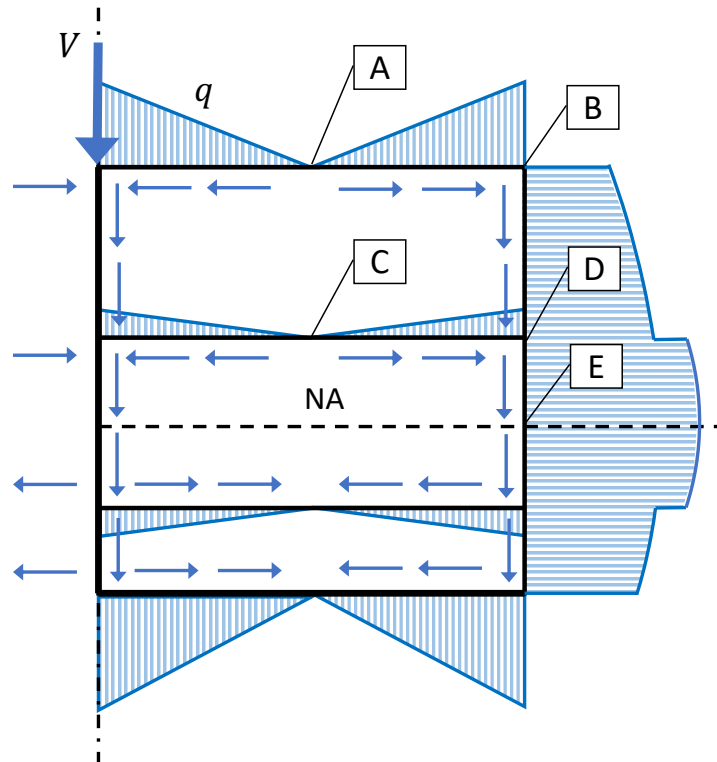


Figure C.14: Hull girder half-section shear flow distribution. The maximum shear flow value is located at the neutral axis. The value at the bulkhead is twice that of the side shell plates. Since the bulkhead is also twice as thick as the side shell plates, the maximum shear stress values are equal.

where $\|\cdot\|$ denotes the 2-norm. However, we cannot evaluate the above integral precisely. Instead, we use the approximation

$$A_S \approx 2\varphi_A L l_T^{\text{mid}}, \quad (\text{D.1})$$

where l_T^{mid} is the midship arc length from keel centerline to hull waterline and φ_A is a correction factor that accounts for the narrowing hull towards the forward and aft of amidships. The arc length is

$$l_T^{\text{mid}} = \int_0^{B/2} \left\| \left[-\frac{dz^{\text{mid}}(x)}{dx} \right] \right\| dx = \int_0^{B/2} \sqrt{1 + \left(\frac{2}{B} \right)^{2\beta} (T\beta)^2 x^{2\beta-2}} dx, \quad (\text{D.2})$$

where $z^{\text{mid}}(x)$ is z-coordinate of the hull at amidships at offset x . By writing $x = H^{\text{fore}}(L/2, z)$ from (14) with respect to z , we obtain $z^{\text{mid}}(x) = T(2x/B)^\beta$.

The integral (D.2) can be evaluated exactly for only a few β values. We deal with the general case by substituting the integrand function with an interpolating polynomial. A cubic polynomial is sufficiently accurate because the integrand is smooth and curves only in one direction. Integration using a cubic polynomial (known as Simpson's 3/8 rule) yields

$$l_T^{\text{mid}} \approx \frac{B}{16} \sum_{k'=0}^3 S_{k'+1} g^{\text{mid}}(k'B/6), \quad (\text{D.3})$$

where g^{mid} is the integrand function in (D.2) and $S = (1, 3, 3, 1)$ is the vector of Simpson's multipliers.

The integrand g^{mid} evaluated in (D.3) is a posynomial raised to a fractional power and thus not log-convex. Next, we introduce auxiliary variables and an inequality constraint to obtain an equivalent log-convex form. Using the auxiliary variables $r_{k'}^g$, $k' = 0, \dots, 3$ we can now write (D.1) as the pair of valid posynomial inequalities

$$A_S \geq 2L\varphi_A \sum_{k'=0}^3 S_{k'+1} \sqrt{r_{k'}^g}, \quad (\text{D.4})$$

$$r_{k'}^g \geq 1 + \left(\frac{2}{B} \right)^{2\beta} (T\beta)^2 \left(\frac{k'B}{6} \right)^{2\beta-2}, \quad k' = 0, \dots, 3. \quad (\text{D.5})$$

References

Agrawal, A., Diamond, S., Boyd, S., 2019. Disciplined geometric programming. *Optimization Letters* 13, 961–976.

AS Tallink Grupp, 2025. Annual report.

Boyd, S., Kim, S.J., Vandenberghe, L., Hassibi, A., 2007. A tutorial on geometric programming. *Optimization and Engineering* 8, 67–127.

Boyd, S., Vandenberghe, L., 2004. Convex Optimization. Cambridge University Press.

Boyd, S.P., Kim, S.J., Patil, D.D., Horowitz, M.A., 2005. Digital circuit optimization via geometric programming. *Operations Research* 53, 899–932.

Chiang, M., Tan, C.W., Palomar, D.P., O’neill, D., Julian, D., 2007. Power control by geometric programming. *IEEE Transactions on Wireless Communications* 6, 2640–2651.

Christiansen, M., Fagerholt, K., Nygreen, B., Ronen, D., 2007. Maritime transportation. *Handbooks in Operations Research and Management Science* 14, 189–284.

Christiansen, M., Hellsten, E., Pisinger, D., Sacramento, D., Vilhelmsen, C., 2020. Liner shipping network design. *European Journal of Operational Research* 286, 1–20.

Diamond, S., Boyd, S., 2016. CVXPY: A Python-embedded modeling language for convex optimization. *Journal of Machine Learning Research* 17, 2909–2913.

Domahidi, A., Chu, E., Boyd, S., 2013. ECOS: An SOCP solver for embedded systems, in: 2013 European Control Conference (ECC), IEEE. pp. 3071–3076.

Duffin, R.J., Peterson, E.L., Zener, C., 1967. Geometric Programming – Theory and Application. John Wiley & Sons.

Havre, H.F., Lien, U., Ness, M.M., Fagerholt, K., Rødseth, K.L., 2022. Cost-effective planning and abatement costs of battery electric passenger vessel services. *Transportation Research Part D: Transport and Environment* 113, 103495.

Havre, H.F., Lien, U., Ness, M.M., Fagerholt, K., Rødseth, K.L., 2024. Network design with route planning for battery electric high-speed passenger vessel services. *European Journal of Operational Research* 315, 102–119.

Hoburg, W., Abbeel, P., 2014. Geometric programming for aircraft design optimization. *AIAA Journal* 52, 2414–2426.

Hoburg, W., Kirschen, P., Abbeel, P., 2016. Data fitting with geometric-programming-compatible softmax functions. *Optimization and Engineering* 17, 897–918.

Hollenbach, K.U., 1998. Estimating resistance and propulsion for single-screw and twin-screw ships. *Ship Technology Research* 45.

Kersey, J., Popovich, N.D., Phadke, A.A., 2022. Rapid battery cost declines accelerate the prospects of all-electric interregional container shipping. *Nature Energy* 7, 664–674.

Lloyd’s Register, 2023. Additional calculation procedures for longitudinal strength.

Mittelstedt, C., 2021. *Structural Mechanics in Lightweight Engineering*. Springer.

Moon, H.S., Park, W.Y., Hendrickson, T., Phadke, A., Popovich, N., 2025. Exploring the cost and emissions impacts, feasibility and scalability of battery electric ships. *Nature Energy* 10, 41–54.

Nesterov, Y., Nemirovskii, A., 1994. *Interior-Point Polynomial Algorithms in Convex Programming*. SIAM.

Panasonic, 2024. Primary Lithium Batteries. Technical Report. Panasonic Energy Co Ltd.

Rana, K., Vickson, R., 1991. Routing container ships using Lagrangean relaxation and decomposition. *Transportation Science* 25, 201–214.

Ritari, A., Mouratidis, P., Tammi, K., 2023. Design optimization of battery-electric marine vessels via geometric programming. *IEEE Access* 11, 76563–76580.

Statistics Finland, 2025. Passenger traffic between Finland and foreign countries by port and country.

Suri, G., Onori, S., 2016. A control-oriented cycle-life model for hybrid electric vehicle lithium-ion batteries. *Energy* 96, 644–653.

Torjuul, C.H.O., 2024. Decision Support for Battery Integration on Feeder Container Vessels. Master's thesis. Norwegian University of Science and Technology.

Ueckerdt, F., Bauer, C., Dirnaichner, A., Everall, J., Sacchi, R., Luderer, G., 2021. Potential and risks of hydrogen-based e-fuels in climate change mitigation. *Nature Climate Change* 11, 384–393.

Varsta, P., Remes, H., Romanoff, J., 2017. Global hull-girder response (quasi-static, prismatic beam models), in: Carlton, J., Jukes, P., Sang, C.Y. (Eds.), *Encyclopedia of Maritime and Offshore Engineering*. John Wiley & Sons.

Watson, D.G.M., Gilfillan, A.W., 1977. Some ship design methods. *Naval Architect* 4.